Title
Micromechanics of Human Bone: Role of Architecture and Tissue Material Properties

Author
Sadoughi, Saghi

Publication Date
2019

Peer reviewed|Thesis/dissertation

Micromechanics of Human Bone: Role of Architecture and Tissue Material Properties

by

Saghi Sadoughi

A dissertation submitted in partial satisfaction of the

requirements for the degree of

Doctor of Philosophy

in

Engineering – Mechanical Engineering

in the

Graduate Division

of the

University of California, Berkeley

Committee in charge:

Professor Tony M. Keaveny, Chair
Professor Lisa Pruitt
Professor Lin Lin

Fall 2019

Micromechanics of Human Bone: Role of Architecture and Tissue Material Properties

Abstract

Micromechanics of Human Bone: Role of Architecture and Tissue Material Properties

by

Saghi Sadoughi

Doctor of Philosophy in Engineering – Mechanical Engineering

University of California, Berkeley

Professor Tony M. Keaveny, Chair

Knowledge of the biomechanical behavior and failure mechanisms of human bone is fundamental to understanding the etiology of bone fractures as well as the mechanisms by which aging, disease, and treatment can alter the mechanical competence of bone. In this context, the focus of this dissertation was to enhance the current understanding of the biomechanical mechanisms of bone strength, and more specifically, to elucidate the role of architecture and tissue material properties in overall bone strength and whole-bone failure behavior.

Using the latest advances in micro-computed tomography and high-resolution finite element modeling, we investigated the effect of typical population-variations in tissue-level ductility on human vertebral strength. We found that compared to the reference case, varying both cortical and trabecular tissue ultimate strains by ±1 SD from their mean values changed vertebral strength by at most ±8%, an effect that was relatively uniform across all the specimens. Overall strength changed similarly for similar (±1 SD) changes in trabecular versus cortical ductility. Further analysis revealed that only a tiny proportion of tissue failed (< 2%) when the whole bone reached its point of structure-level failure, and that the failure mode and location of this tiny amount were relatively insensitive to typical variations in tissue ductility. These findings suggest that it is the overall load transfer within the whole vertebral body —determined by bone volume fraction and microstructure— that dictates where failure occurs rather than typical variations in the ductility of the tissue. Together these findings suggest that typical variations in tissue ductility might have a relatively modest impact on vertebral strength compared to the multiple-fold variations in vertebral strength that are typically observed across any elderly population.

Combining micro-computed tomography, high-resolution finite element modeling and biomechanical testing, we sought to provide further insight into the tissue modulus of trabecular

bone and better elucidate its relation with bone volume fraction and trabecular microarchitecture. Our results indicated that effective tissue modulus of vertebral trabecular bone varied greatly among the specimens and was negatively correlated with bone volume fraction of each vertebra ($R^2 = 0.51$, $p < 0.05$). These results suggest that there can be 3X variation in tissue modulus across the elderly human vertebrae, about 50% of which may be explained by variations in bone volume fraction. Together these findings suggest that as trabecular bone becomes older and thus more porous due to an imbalance between bone formation and resorption, the tissue may become stiffer to compensate for the bone loss.

The work presented in this dissertation has also provided substantial insight into the structure–function relations for trabecular bone from different anatomic sites. We investigated the main structure–function relation —characterized by bone volume fraction versus on-axis yield stress— for human calcaneal trabecular bone and compared this relation to that for trabecular bone from other anatomic sites. We found that the relation between yield stress and bone volume fraction of the calcaneus was most similar to that of the proximal tibia. Furthermore, our results demonstrated that while there was no universal yield stress–bone volume fraction relation for trabecular bone across different anatomic sites for on-axis loading, the general (normalized) yield stress–bone volume fraction relation was similar for all sites. This similarity in the normalized relation suggests that a given percentage deviation from the mean bone mass has the same mechanical consequence at the calcaneus as it does at the other anatomic sites.

In closure, this dissertation provides answers to some of the fundamental questions regarding the role of architecture and tissue material properties in explaining the variations in overall bone strength across individuals, and provides new insight into the etiology of age-related fractures. This work also outlines potential areas of future research to further advance our current understanding of overall bone strength and fracture etiology.

To Mom and Dad

Contents

List of Figures

List of Tables

Acknowledgements

There are so many people who have contributed in small and big ways to this work, without whom my PhD journey would not have been as rewarding and joyful.

First, I would like to thank my research advisor, Tony Keaveny, who by giving me the opportunity to work in the Orthopedic Biomechanics Laboratory, forever changed my life and career for the best. Without his guidance, insight, enthusiasm, and expertise I would have never been able to complete this degree. I feel incredibly fortunate to have had the opportunity of doing research under his supervision.

Second, I would like to acknowledge my Berkeley Professors, Lisa Pruitt and Lin Lin for serving as members of my qualifying exam and dissertation committees.

Third, I would like to thank all the past and present members of the Orthopedic Biomechanics Laboratory for making the lab a fun and supportive place to work. I would especially like to thank Megan Pendleton. She has been a wonderful friend and lab mate, and I cannot thank her enough for the endless hours of discussion about research and life in general (and of course, for our Menchie's breaks!). I am so grateful for Noah Bonnheim. He has also been a wonderful friend and lab mate. I have enjoyed every moment of working and travelling to conferences with him and I am really going to miss his companionship. I owe a great deal of thanks to Shashank Nawathe for helping me get started at the OBL, and Aaron Fields for always being eager to aid me in troubleshooting problems. I would also like to thank Shannon Emerzian for everything that comes with sitting next to me for four years; Tongge Wu, Bo Yang, and Emily Lindberg for being my windsurfing buddies (yes, it is possible to have hobbies other than research at grad school!); Semih Bezci for being a great source of entertainment!; and all the other members of the Biomechanics Lab for the great memories. I have had the pleasure of working with a number of undergraduate students, among whom, Shan Zhu and Ariana Moini have been critical in the development of essential techniques and performing the analyses.

On a more personal note, I would very much like to thank my friends from life outside of grad school who have been the best support network: Niloofar Piroozi for always being an ear for me regardless of the three-hour time difference; Fatemeh Rahimian and Zahra Aghaee for making me believe that true friendships do not fade away even when you are thousands of miles apart; and Ali Ameri for being the best companion for this journey and for teaching me how to see life more beautifully.

Last, but not the least, I owe endless thanks to my family for their unconditional love and support. To my mom and dad, for providing all the opportunities I had and for inspiring me to never give up on my dreams; to my sister, for always watching out for the little one; to my grandparents for always supporting me and being proud of me; and to my dear uncle Saeed, for being a great source of joy and positive energy, and for always showing me how much he cares about me and is proud of me. I'm so grateful for having every single one of them in my life.

1. Introduction

While the skeletal system in a healthy individual is well adapted for performing a range of activities, its function can be compromised by aging or disease. One of the most prevalent skeletal diseases is osteoporosis, which results from an imbalance in bone remodeling [1]. Osteoporosis is characterized by low bone mass and microarchitectural deterioration of bone tissue (**Figure 1-1**), with a consequent increase in bone fragility and risk of fracture [2]. According to the National Osteoporosis Foundation, over 2 million osteoporosis-related fractures occur annually in the United States. The most common sites for fracture are the vertebral body (550,000 annually), the distal radius (400,000 annually), and the proximal femur (300,000 annually) [3]. Osteoporotic fractures can decrease the quality of life due to the associated pain and subsequent disability. They can even cause early mortality: 28% of spine-fracture patients and 22% of hip-fracture patients die within one year following the fracture [4]. Besides all the burden, osteoporosis is costly. For US alone, the estimated cost of osteoporosis is $19 billion per year [3]. As the size of the aging population increases, osteoporosis prevalence and the associated costs are projected to rise dramatically in the coming years. Therefore, osteoporosis is considered a major public health threat and its diagnosis is critical.

The World Health Organization defines osteoporosis by an areal bone mineral density (BMD) measurement —made with dual energy X-ray absorptiometry (DXA)— that is 2.5 standard deviations below that of a sex-matched healthy young adult [5], and the current clinical assessment of osteoporosis is based on this definition. However, since the clinical outcome of osteoporosis is bone fracture, attention is now increasingly focused towards identification of patients at high risk of fracture rather than identification of people with osteoporosis defined by the BMD criteria alone. This is because not all the individuals who experience fractures are identified as being osteoporotic by the BMD criteria, many of them are indeed osteopenic [6], and therefore, miss being considered for preventative treatment. This indicates that BMD alone, which is a measure of bone quantity, is not enough in identifying individuals at risk of fracture. It also suggests that fracture risk may depend on bone quality, which comprises all the other factors, such as morphology (size/shape), micro-architecture and material properties (**Figure 1-2**, [7]). Aside from this, DXA scanning is

under-utilized as many patients do not get tested (Zhang et al., 2012). Therefore, seeking alternative modalities that are more widely available than DXA and can provide information in addition to bone quantity might help better identify individuals at risk of fracture. In this context, the goal of this dissertation was to elucidate the effect of bone tissue material properties (a bone quality factor) on its overall strength. Furthermore, it sought to investigate and provide insight into the use of other diagnostic modalities in the assessment of osteoporosis.

The remainder of this chapter is intended to establish a foundation in bone biomechanics, which will be useful in understanding the material presented in the subsequent chapters of this dissertation. First, the structure and composition of bone will be discussed, followed by descriptions of morphology and mechanical behavior of human trabecular and cortical bone. Then, contemporary issues regarding computational modeling of whole bones such as vertebral body and proximal femur will be addressed. The objectives and scope of this dissertation will be outlined in the final section.

1.1. Structure and Composition of Bone*

Bone is a hierarchical composite material, consisting of distinct structures that vary in size from a few nanometers to tens of millimeters (**Figure 1-3**). By weight, the constituent materials of bone are inorganic ceramic materials (primarily hydroxyapatite, 60%), organic materials (primarily type I collagen, 30%), and water (10%). At the smallest size-scale, the hydroxyapatite crystals typically form small plate-like structures with dimensions on the order of 5 × 15 × 40 nm. These crystals are surrounded by woven collagen fibrils (~30 nm diameter × 300 nm length). At the next hierarchical scale (~10 μm), the mineralized collagen fibrils are arranged in two distinct forms. In the first form, the fibrils orient in a random fashion to form a structure often termed woven bone. In the second form, the fibrils take a more organized form and assemble in unidirectional sheets called lamellae, which then stack together with alternating fiber directions in each layer.

* This section was adapted in part from [58].

Lamellae are arranged in five different structures at the next scale. The first structure is called a lamellar packet. The lamellae in these packets are not well organized. However, lamellar packets come together at the next scale to form a highly organized lattice of rod- and plate-like structures called trabecular bone (also known as cancellous or spongy bone). Trabecular bone is a highly porous structure (> 60% porous in humans; **Figure 1-4**) that is found in the end of long bones (such as the femur) and in irregularly shaped bones (such as the vertebral body). The other four hierarchical structures formed by lamellae are primary lamellar, Haversian (osteonal), laminar, and woven bone. Primary lamellar bone is new bone that consists of the large concentric rings of lamellae that circle the outer 2-3 mm of the diaphysis of long bones. Haversian or osteonal bone consists of approximately 10-15 lamellae, arranged in concentric cylinders (~200 μm diameter and 2 mm length) about a central Haversian canal (a canal about 50 microns in diameter), in which blood vessels, nerves, and bone cells reside. The substructure of the concentric lamellae is termed an osteon. Osteons are the primary discrete units of human cortical bone. Laminar bone consists of a series of concentric laminae (each laminae is ~0.1-0.2 mm thick) around a marrow cavity. Sandwiched between adjacent laminae is a two-dimensional network of blood vessels. Woven bone is found in areas of rapid growth such as at locations of fracture.

The primary difference, therefore, between the cortical and trabecular bone is the open cellular structure of the latter. The actual bone tissue at the underlying hierarchical level is very similar, being made of lamellar bone. However, one difference does exist. Bone is a biologically active material that is capable of adapting to its mechanical environment, and is continually in the process of removing old or damaged tissue and replacing it with new tissue. This remodeling process consists of bone tissue being removed by osteoclast bone cells and new tissue being formed by osteoblast cells. This process is thought to be governed by mechano-sensitive bone cells called osteocytes, which reside alone in small elliptical holes in the bone tissue called lacunae (5-8 mm diameter). There is more bone remodeling on the free surfaces of the rods and plates within the trabecular bone than on the internal surfaces of Haversian canals within the cortical bone. Therefore, trabecular bone tends to be slightly less mineralized than cortical bone. The details of trabecular and cortical morphology and material and mechanical properties will be addressed in the next section.

1.2. Mechanical Behavior of Bone

The mechanical behavior of bone is determined by bone quantity as well as bone quality factors including morphology (size/shape), cortical and trabecular microstructure, and tissue material properties. Measures of bone mass or density, such as bone volume fraction or bone mineral density, are strong predictors of bone strength [8–12]. However, these measures do not completely explain variations in bone strength. Factors that contribute to bone strength but are not accounted for by measures of bone density or mass are termed bone quality factors (**Figure 1-2**) [7]. In other words, two bone specimens that have the same density but different strengths are considered to have different quality. As such, better characterization of bone quality factors is fundamental in improving our understanding of bone strength and fracture risk assessment.

Proper measurement of the tissue material properties —one of the aforementioned bone quality factors— is central to understanding the effects of treatment, aging, and disease on bone fragility at the tissue level as well as the integrated effects at higher scales. For example, antiresorptive drug therapies can considerably reduce fracture risk [13,14], yet the biomechanical effects of these therapies on bone tissue are not clear [7]. Furthermore, tissue material properties are essential inputs to computational [15–17] and theoretical models [18] of bone. Chapter three of this dissertation is devoted to the topic of combining experimental and computational techniques to determine vertebral trabecular hard tissue properties.

One poorly understood but potentially important bone tissue material property is tissue-level ductility, which can be characterized by the amount of post-yield deformation of the tissue between yielding and fracture. This bone-quality factor is known to decrease with age for cortical tissue [19], and varies appreciably across the population for trabecular tissue (**Figure 1-5**) [20,21]. To date, only a few studies have measured the ductility for either trabecular or cortical tissue, due to the technical challenges associated with ductility testing of small samples of bone tissue [22]. The limited data so far indicate that trabecular tissue is four-fold more ductile than cortical tissue [19,20]. Therefore, the distinction between cortical and trabecular tissue ductility could potentially be important in determining their individual roles in whole-bone failure behavior, and the etiology

of osteoporotic fractures. Chapter two of this dissertation is devoted to investigating the effect of variations in tissue-level ductility on vertebral strength.

The remainder of this section contains a brief overview on morphology and mechanical properties of trabecular and cortical bone.

1.2.1. Trabecular Bone

Trabecular bone is a network of small, interconnected rods and plates, called trabeculae, with relatively large spaces between them. Typical thickness of individual trabeculae is in the range of 100-300 μm in human bone, and typical intertrabecular spacing is on the order of 500-1500 μm [23]. The porosity of trabecular bone (typically 50-95%) is dominated by the spaces between individual trabeculae. Trabecular bone morphology and mechanical properties can vary greatly with age, anatomic site (**Figure 1-6**), and between individuals. However, most of the variations in morphology and mechanical properties can be described by bone volume fraction (BV/TV, the fraction of the total volume that is occupied by the trabecular hard tissue) or bone density (ρ, the ratio of bone mass to total volume). These two properties are related by the density of the trabecular tissue ($\rho_{tissue} = \frac{\rho}{BV/TV}$), which is relatively constant for healthy adults [24].

The apparent compressive stress–strain behavior of trabecular bone is typical of a class of porous materials called cellular solids (**Figure 1-7**; the term "apparent" refers to properties measured at the continuum level of a whole trabecular structure, as opposed to "tissue" properties that are measured at the level of individual trabeculae). It displays an approximately linearly elastic region followed by a local peak, and then a strain-softening or plateau region of near constant stress with increasing strain. Tensile behavior is more brittle, with fracture occurring at relatively low strains. Trabecular bone also exhibits tension-compression strength asymmetry —yield and ultimate strengths in compression are typically larger than in tension [10,25–27]. Most importantly, for trabecular bone, the stiffness and strength depend on its apparent density and can vary by two orders of magnitude within the same metaphyseal region. In fact, apparent density (or BV/TV) is

the most important factor for determining trabecular bone mechanical properties: 70-90% of the variations in strength within a single anatomic site can be explained by apparent density [8–10,28]. Depending on the trabecular architecture, modulus or strength vary with apparent density (or BV/TV) by a linear relation or a power law relation with an exponent of 1-3. Chapter four of this dissertation is devoted to investigating these structure–function relations for trabecular bone from different anatomic sites. More specifically, the strength-BV/TV relation of human calcaneal trabecular bone is studied and compared to that of other anatomic sites with the goal of providing insight into the use of calcaneal measurements in osteoporosis assessment of other anatomic sites.

1.2.2. Cortical Bone*

Cortical bone is a solid-like structure that contains a series of voids having dimensions about 200 μm or less (Haversian canals, Volkmann's canals, resorption cavities, lacunae, and canaliculi). It has a porosity of less than about 30 percent, or equivalently, a volume fraction of greater than about 0.70. In contrast to trabecular bone, the apparent density (or BV/TV) of human cortical bone varies little from site to site. This smaller variation results in a much less heterogeneity in cortical bone's material properties compared to trabecular bone.

Human cortical bone is generally assumed to be transversely isotropic, meaning that it has one primary material axis (the longitudinal direction) and is isotropic in the plane perpendicular to this axis (the transverse plane). The longitudinal axis is generally aligned with the diaphyseal axis of long bones. Cortical bone is both stronger and stiffer when loaded in the longitudinal direction, compared with the radial or circumferential directions. This structure efficiently resists the largely uniaxial stresses that develop along the diaphyseal axis during habitual activities such as walking and running. In addition to having anisotropic elastic and strength properties, cortical bone also has asymmetric strengths: it is stronger in compression than tension for each principal material direction (**Figure 1-8**). When loaded to failure in a monotonic test, human cortical bone exhibits an initial linear elastic behavior, a marked yield point, and failure at a relatively low strain level.

* This section was adapted in part from [58].

Unlike the ultimate stresses which are higher in compression, ultimate strains are higher in tension for longitudinal loading (**Figure 1-8**). In contrast to its longitudinal tensile behavior, cortical bone is relatively brittle in tension for transverse loading and brittle in compression for all loading directions.

1.3. Finite Element Modeling

Finite element analysis is a powerful computational tool for investigating the biomechanical behavior of bone. This technique allows researchers to perform "virtually real" experiments that have several advantages over the gold-standard biomechanical tests. First, the technique is non-destructive, so the effects of variables such as boundary and loading conditions [29,30] or material properties [31–33] can be evaluated in controlled parameter studies. Second, the technique can provide detailed insight into stress and strain distributions within the bone [34–36], whereas biomechanical testing only yields information about the apparent-level mechanical behavior (or at best, about local stresses and strains on the surface of the vertebra using strain gauges [37]. Perhaps the greatest benefit of finite element modeling in bone mechanics research lies in combining the technique with biomechanical testing in order to leverage the individual strengths of each approach. Using this combined approach, researchers have gained substantial insight into tissue-level mechanical properties and failure mechanisms [17,38,39].

This dissertation reports on the use of high-resolution finite element modeling of whole vertebral bodies. The finite element models were constructed from micro-CT images (37 μm spatial resolution) of vertebral bodies by converting each voxel in the images into an eight-noded brick element [39]. Hence, the models implicitly captured the spatially heterogeneous microarchitecture, the thin cortical shell, and the porous endplates of the vertebra (**Figure 1-9**). By accurately capturing the physics of these microstructures, the models can be used to provide detailed insight into the micromechanics of the vertebral body and the underlying failure mechanisms.

In contrast to continuum-level finite element models based on quantitative-CT images (1-3 mm spatial resolution) in which each element is assigned a different material property based on its CT-derived density [40–45], high-resolution finite element models typically use homogeneous and isotropic material properties. This enables separation of the effects of variations in microarchitecture from the effects of variations in material properties. Additionally, apparent-level predictions of mechanical properties as well as tissue-level stress and strain distributions from high-resolution finite element models with homogeneous and isotropic material properties have correlated well with experimental measures providing some level of validation for this modeling approach [15,17,46–49].

Computationally, high-resolution finite element modeling of whole vertebra requires both state-of-the-art software and hardware. In the past, high-resolution finite element models of trabecular bone have traditionally been solved with the iterative, element-by-element (EBE) preconditioned conjugate gradient (PCG) method [36,39,46,48]. This method is memory efficient and the work per iteration and per degree of freedom is constant. However, because the number of iterations required to reduce the residual by a constant amount using the EBE-PCG method rises dramatically as the problem size increases, this method is inefficient for solving larger problems, such as those involving the whole vertebra. Whole vertebral models typically contain on the order of 300 million degrees of freedom, and therefore, their analyses require more efficient solvers [50–52] and substantial parallel computing capacity. By dividing the global finite element mesh into sub-domains and spreading the workload over thousands of processors that perform the computations in parallel, previously intractable problems can be solved in minutes. The work in this dissertation utilizes a highly-scalable, implicit finite element framework (*Olympus* [50,52]) implemented on some of the world's fastest and most advanced parallel supercomputers. In particular, the work has utilized implementations of *Olympus* on three supercomputing platforms: 1) a Sun Constellation cluster with 62,976 processors and 123 TB of memory (Ranger; Texas Advanced Computing Center, Austin, TX USA); 2) a Dell Power Edge C8220 cluster with 102,400 dual 8-core Intel Xeon E5-2680 processors and 270 TB of memory (Stampede; Texas Advanced Computing Center, Austin, TX USA); and 3) a Dell cluster with 4,200 68-core Intel Xeon Phi 7250 ("Knights Landing") and 470 TB of memory plus 1,736 48-core Intel Xeon Platinum 8160 ("Skylake")

processors and 330 TB of memory (Stampede2; Texas Advanced Computing Center, Austin, TX USA).

In addition to their large size, high-resolution finite element models of whole vertebrae represent a significant computational challenge due to their numerical complexity. For example, performing fully nonlinear analysis involves both material and geometric nonlinearities. Material nonlinearities are necessary in order to capture the tension-compression strength asymmetry of the bone tissue [15,23]. Geometric nonlinearities are required to capture the deformation mechanisms such as large-deformation bending and buckling [17,53]. Due to the computational challenge of simulating these nonlinearities, past studies on whole bone specimens have mostly focused on *linear* analysis [30,34–36]. However, recent advances in supercomputing technology combined with efficient solver algorithms [50,52] have finally made it possible to perform fully *nonlinear*, high-resolution finite element analysis of whole bone specimens [54–57]. Chapters two and three of this dissertation are devoted to such analyses.

1.4. Objectives and Scope

The overall goal of this dissertation is to enhance the current understanding of the biomechanical mechanisms of whole-bone strength and etiology of osteoporotic fractures. More specifically, the first objective is to elucidate the effect of tissue material properties on whole-bone strength, a potentially important factor in fracture risk assessment. The second objective is to provide insight into the potential use of diagnostic modalities that are more widely available than DXA in assessment of osteoporosis.

Chapter two explores the effect of typical population-variations in tissue-level ductility on human vertebral strength. By simulating multiple combinations of cortical and trabecular tissue ultimate strain values for each vertebral body, this study provides insight on how the uncertainty in vertebral strength due to the unknown degree of tissue-level ductility compares to variations in vertebral

strength across the population and whether taking into account this uncertainty might improve fracture risk assessment.

Chapter three reports on the effective tissue modulus of human vertebral trabecular bone. In a novel approach that combines experimental and computational methods and accounts for the unknown degree of tissue-level ductility, this study uses strength measurements of whole-bone vertebral specimens to provide estimates for the effective tissue modulus of human vertebral trabecular bone. By investigating the correlation between effective tissue modulus and age, bone volume fraction and microstructural parameters of vertebral trabecular bone, this study also seeks to provide insight into the effect of aging, disease and treatment on tissue modulus of vertebral trabecular bone.

Chapter four investigates the structure–function relations for human calcaneal trabecular bone and their comparison with other anatomic sites. With the help of high-resolution non-linear micro-CT based finite element analysis, this study explores how the relation between mechanical properties and microarchitecture of calcaneal trabecular bone compares to that of trabecular bone from other anatomic sites; an insight that could potentially be important in the use of calcaneal measurements —for example made by ultrasound— for osteoporosis assessment at other anatomic sites.

Finally, chapter five provides concluding remarks and suggests future directions of the work presented in this dissertation.

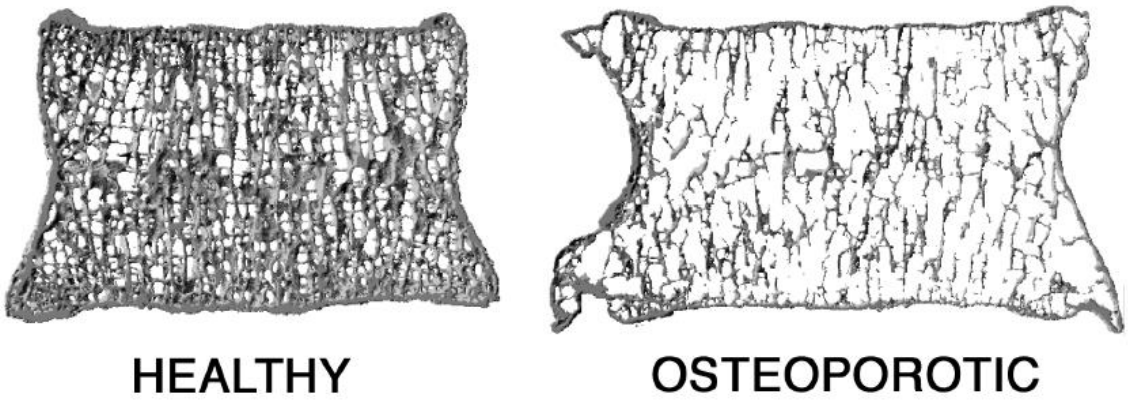

Figure 1-1: Comparison of frontal slices from the vertebra of a healthy individual and an elderly, osteoporotic individual illustrates the decrease in bone mass and deterioration in microarchitecture that occurs with osteoporosis.

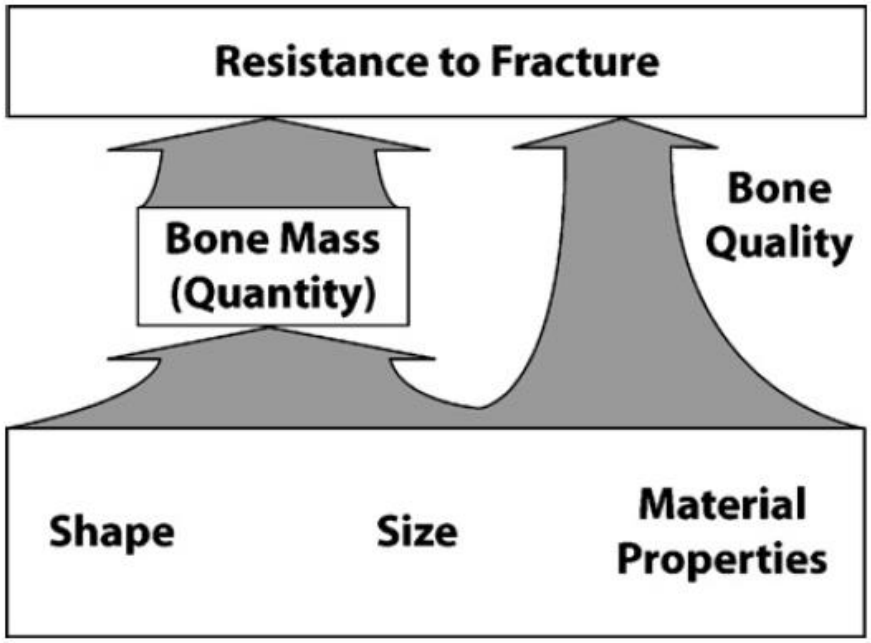

Figure 1-2: Schematic showing the role of bone quality in whole bone strength (resistance to fracture). Factors that contribute to fracture resistance but are not accounted for by bone mass are considered to be quality effects (taken from [7]).

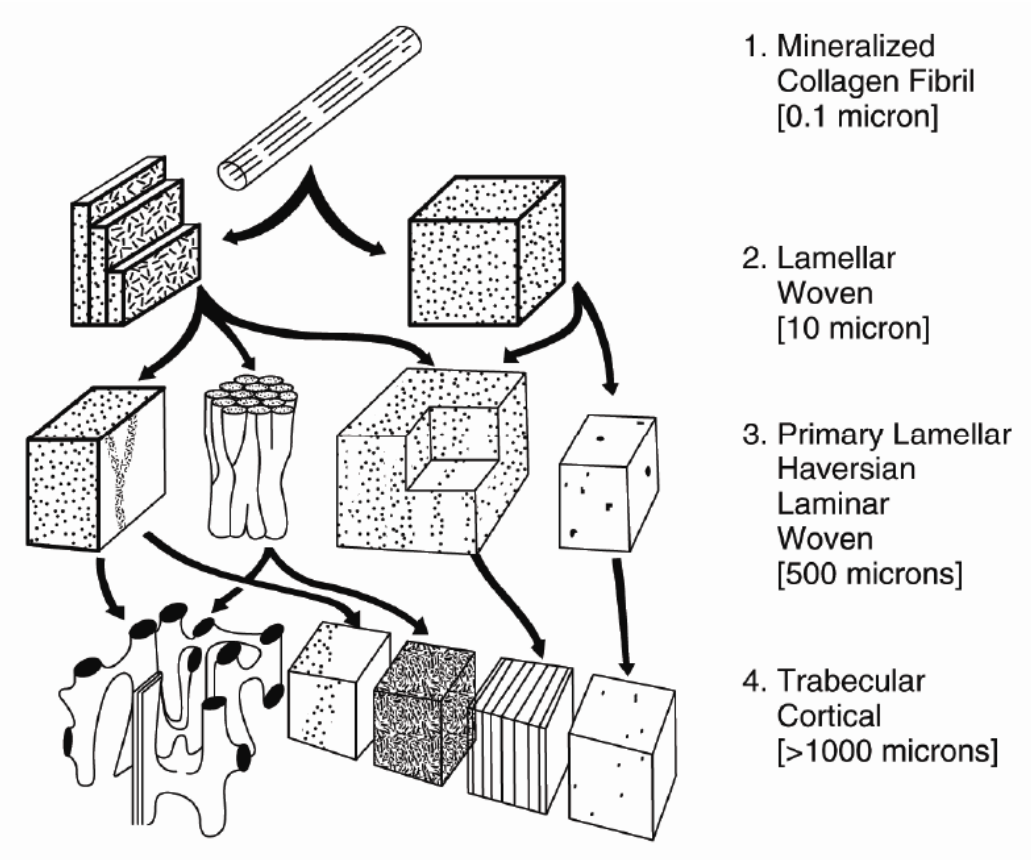

Figure 1-3: Hierarchical structures of bone from the sub-micron length scale to the millimeter length scale (taken from [58]).

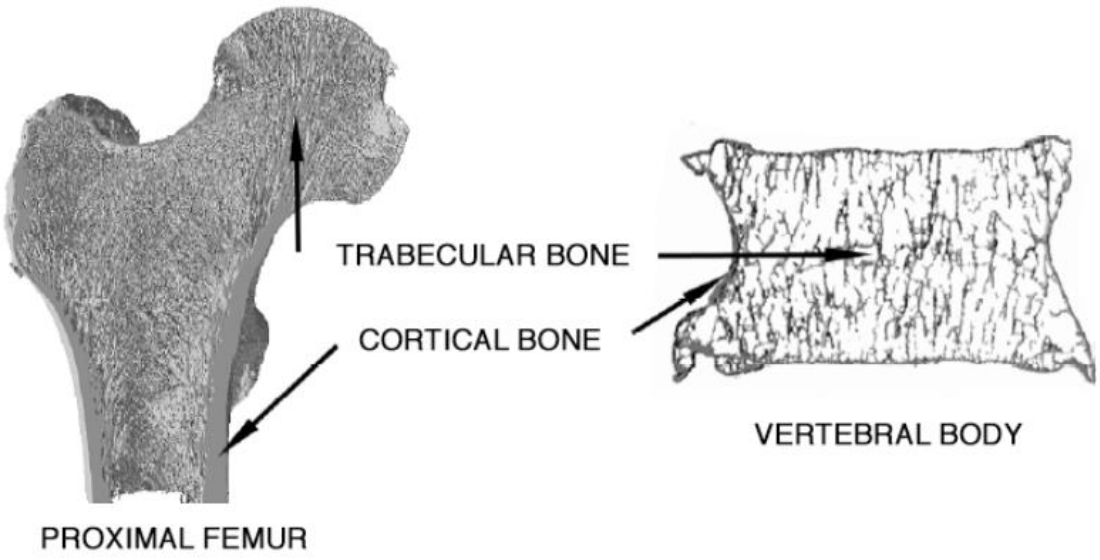

Figure 1-4: Cross-sections of a human proximal femur (left) and thoracic vertebra (right) showing typical arrangements of cortical and trabecular bone.

A.

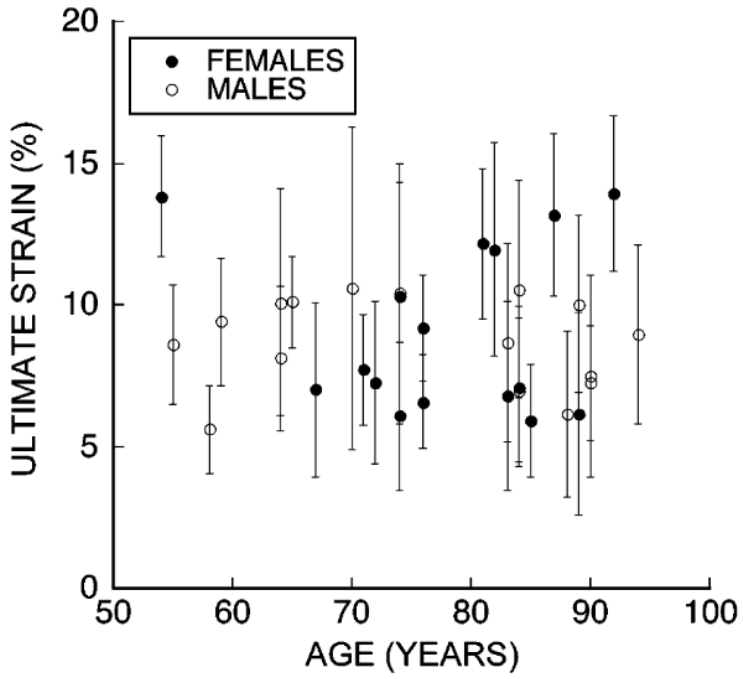

B.

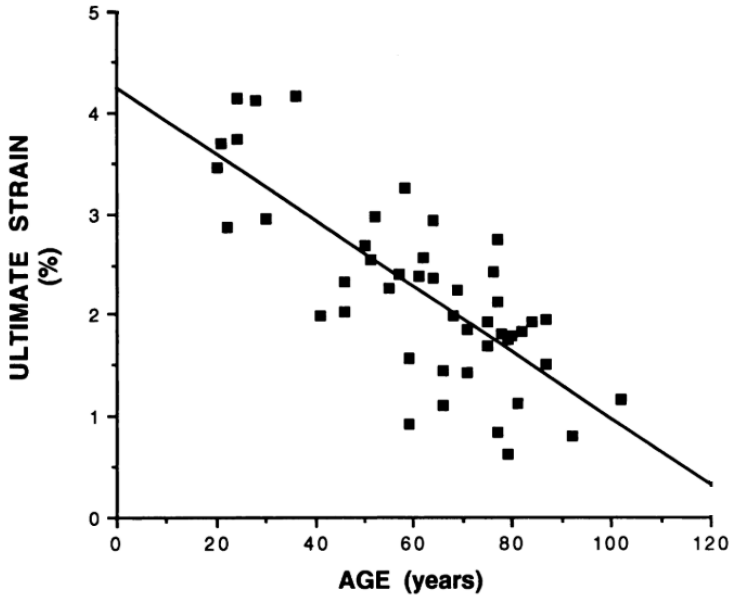

Figure 1-5: Age-related variations in ultimate strain, a measure of tissue-level ductility, for A) trabecular tissue, and B) cortical bone. Ultimate strain decreases with age for cortical tissue [19], but does not show any specific trends for trabecular tissue [20].

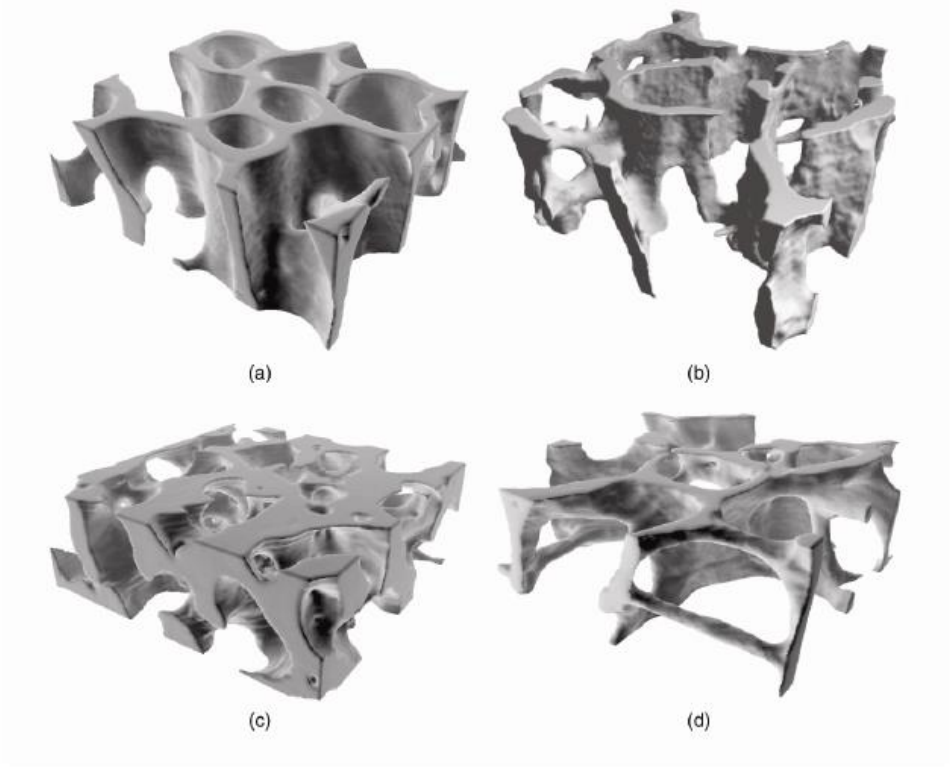

Figure 1-6: High-resolution renderings of trabecular bone from: a) bovine proximal tibia; b) human proximal tibia; c) human femoral neck; d) human vertebra (taken from [58]).

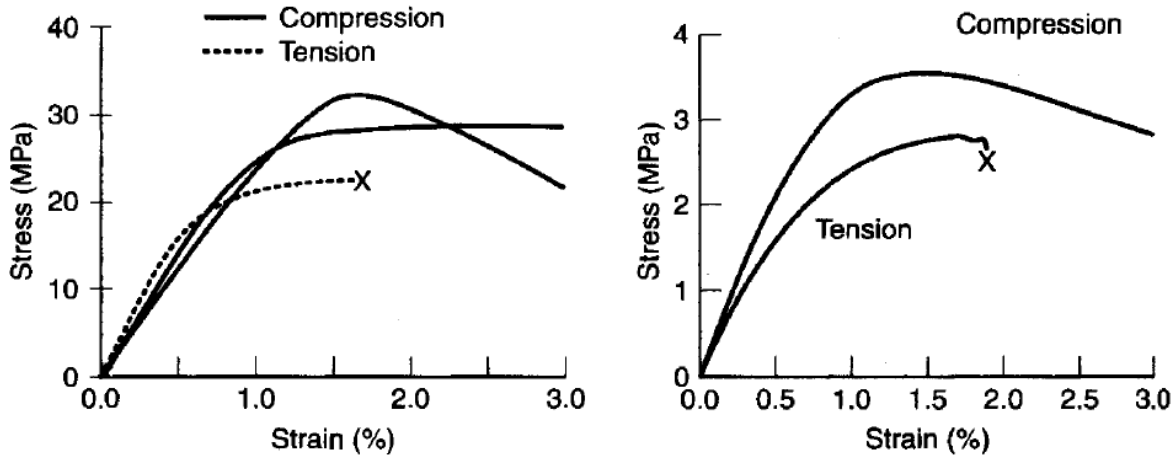

Figure 1-7: Typical stress–strain curves for high-density (left, ρ = 0.65 g/cc) and low density (right, ρ = 0.20 g/cc) trabecular bone. Note that the strength and stiffness of the high-density bone is an order of magnitude greater than that for the low-density bone (taken from [58]).

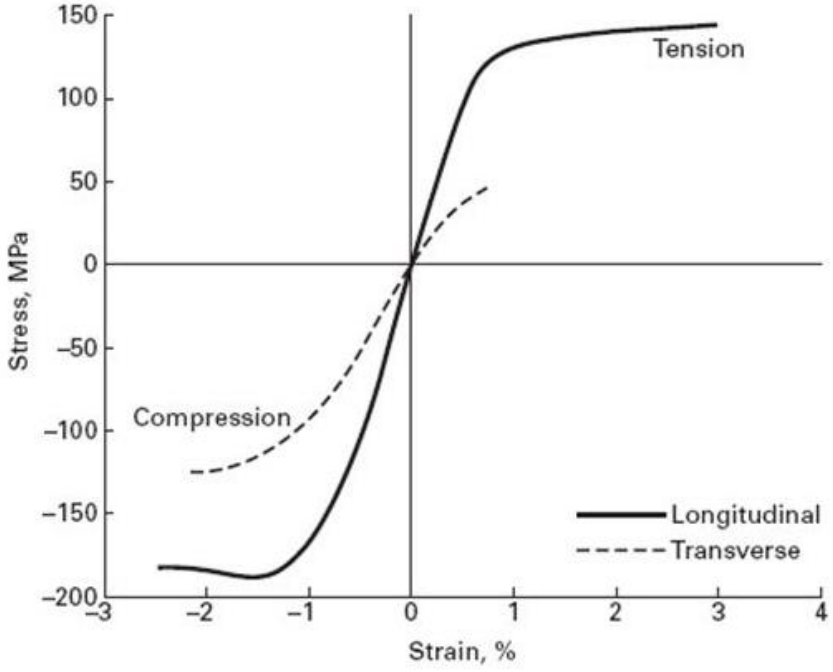

Figure 1-8: Typical stress–strain behavior for human cortical bone. The bone is stiffer in the longitudinal direction, indicative of its elastic anisotropy. It is also stronger in compression than tension, indicative of its strength asymmetry. Cortical bone is relatively ductile for longitudinal tension, but is brittle in all other loading modes (taken from [58]).

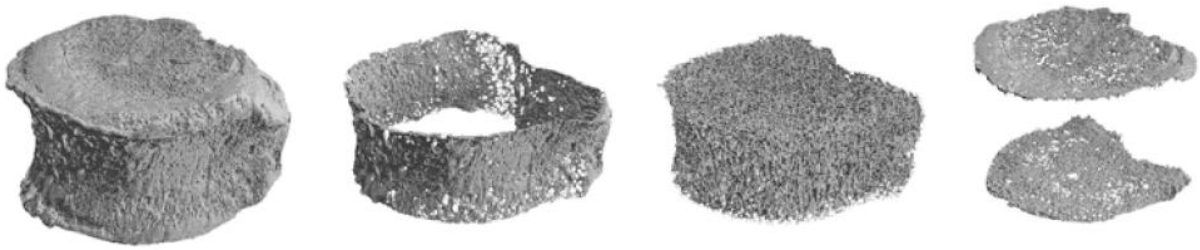

Figure 1-9: Vertebral body compartmentalized (from left to right) into the cortical shell, trabecular centrum, and endplates.

2. Effect of Variations in Tissue-Level Ductility on Human Vertebral Strength

2.1. Introduction

Although the current clinical assessment of osteoporosis relies on a measurement of bone mineral density (BMD) by dual energy X-ray absorptiometry (DXA), many individuals who experience fractures are not identified as being osteoporotic by the BMD criteria [6], and therefore, miss being considered for preventative treatment. This suggests that BMD alone, which is a measure of bone quantity or mass, is not sufficient in identifying individuals at risk of fracture. It also suggests that fracture risk may depend on bone quality, which comprises all the factors other than bone mass, such as morphology (size/shape), micro-architecture and tissue material properties [7]. One tissue material property that is poorly understood but could potentially be an important aspect of whole-bone strength is tissue-level ductility, which can be characterized by the amount of post-yield deformation of the tissue between yielding and fracture. This bone quality factor is known to decrease with age for cortical tissue loaded to failure in tension [19], and varies appreciably across the population for trabecular tissue [20,21]. To date, only a few studies have measured the ductility for either trabecular or cortical tissue due to the technical challenges associated with ductility testing of small samples of bone tissue [22]. The limited data so far indicate that trabecular tissue is four-fold more ductile than cortical tissue [19,20].

Finite element studies on cores of human trabecular bone have shown that the apparent-level strength for fully brittle behavior of the tissue is only about 50% of the strength for fully ductile behavior (Nawathe et al. 2013). Further studies have shown that varying tissue-level failure behavior between the two extreme cases of fully ductile and fully brittle reduces whole-bone strength by 40–60%, an effect that is relatively uniform across all specimens of an anatomic site [54]. However, these studies only simulated the hypothetical extreme cases of tissue ductility, which may not be the actual case across individuals. The more relevant clinical issue is the importance of typical variations in tissue ductility in whole-bone strength and the etiology of

osteoporotic fractures.

To gain additional insight into this issue, we sought to elucidate the effect of typical population-variations in tissue-level ductility on human vertebral strength. Further, we sought to understand the underlying failure mechanisms by which tissue-level ductility influences vertebral strength. To achieve this goal, a parameter study using non-linear micro-CT based finite element analysis was performed on six human vertebrae in which the trabecular and cortical tissue-level ultimate strains were parametrically varied. The specific goals were to: 1) investigate how typical population variations in tissue-level ductility influence whole-bone strength, and 2) whether the effect on whole-bone strength is more significant for variations in trabecular or cortical tissue ductility — potentially important factors in the etiology of age-related osteoporotic fractures.

2.2. Materials and Methods

2.2.1. Specimen Preparation and Imaging

Six human L1 vertebrae (age = 67 ± 15 years, range = 54 – 87 years; n = 4 female, n = 2 male) were used in this study. The specimens were micro-CT scanned at the nominal resolution of 37 μm (Scanco Medical AG, Brüttisellen, Switzerland), thresholded, and coarsened to 74 μm voxel size to facilitate computational analysis. The trabecular and cortical compartments were identified, using a two-dimensional ray-based search algorithm previously developed for the vertebral body ([30], IDL software suite, ITT Visual Information Solutions, Boulder, CO, USA).

2.2.2. Finite Element Analysis (FEA)

Voxel-type finite element models were created for each specimen by converting each voxel into an 8-noded brick element (74 μm element size; [38]), and were subjected to uniaxial compressive loading (**Figure 2-1A**). The material constitutive model, which included kinematic large-deformation geometric non-linearity effects [17], assumed identical tissue-level elastic and yield

properties for both cortical and trabecular tissue, but had different tissue-level ultimate strains for each of the two tissues (**Figure 2-1B**). For each specimen, a complete parameter study was performed in which the ultimate strains for the trabecular and cortical tissue were varied across a range of typical values. All finite elements were assigned the same hard tissue material properties, having an isotropic elastic modulus of 10 GPa, Poisson's ratio of 0.3, and yield strains of 0.69% in compression and 0.33% in tension, respectively [29]. After yielding, the tissue could continue to deform in a plastic manner (with the post yield modulus being 5% of the initial elastic modulus, **Figure 2-1B**) until its strain exceeded the prescribed ultimate strain, at which point the tissue was assumed to have fractured. Assuming the ultimate strain of the bone tissue to be the same in both tension and compression, the post-yield plastic properties varied between each parametric model: three values of cortical ultimate strain (2.2 ± 0.9%, [19]) and three values of trabecular ultimate strain (8.8 ± 3.7%, [20]) for a combination of nine cases per specimen. Two extreme cases of fully ductile and fully brittle were also simulated to provide the theoretical bounds (**Table 2-1**).

To simulate tissue-level fracture, an iterative analysis [54] was performed, in which the overall displacement was applied incrementally. For each incremental displacement step, a fully non-linear finite element analysis was performed that could by itself only simulate element-level yielding, but not fracture. However, after each iteration, strains were computed at each element centroid, and once either the maximum or minimum principal strain at any element centroid exceeded the assumed respective tissue-level tensile or compressive ultimate strain, the element was assumed to have fractured and its elastic modulus was reduced 100-fold to produce an updated model. These updated models were then reloaded, from zero load up to the next displacement increment and the entire process was repeated until the full displacement was applied (**Figure 2-2A**). In this way, an overall non-linear force-deformation curve was generated for the vertebral body that had a local maximum value of applied force, which was defined as the vertebral strength (**Figure 2-2B)**.

Models contained 120 million degrees of freedom on average and were solved using a highly scalable, implicit parallel finite-element framework — Olympus [50,52] running on a Dell Linux Cluster supercomputer (Stampede2, Texas Advanced Computing Center). 2300 CPU hours were

required per incremental step, per case, per specimen, resulting in a total of 11×10^5 used CPU hours.

2.2.3. Outcomes

The main quantitative outcome was the vertebral strength, which was defined as the maximum force on the overall non-linear force-deformation curve (**Figure 2-2B**). To characterize the microstructural failure mechanisms, the proportion of yielded and fractured tissue (at structure-level failure) was quantified based on the number, location (i.e., trabecular versus cortical) and failure modes (i.e., tension versus compression) of the yielded and fractured elements in each model. The total proportion of *yielded tissue* was defined as the number of elements exceeding the assumed tissue-level yield stress divided by the total number of elements in the model (excluding the PMMA). A similar calculation was performed to calculate the proportion of *fractured tissue*. We henceforth adopt the terminology *failed tissue* to denote all the bone tissue that has failed either by yielding or fracture.

A full parameter study was performed for each of the six specimens. To enable comparisons across specimens, results were expressed as a percentage difference with respect to the *reference case* for that specimen, which was defined at the case having the mean values for both trabecular and cortical tissue-level ultimate strains.

2.3. Results

Compared to the reference case, varying both cortical and trabecular tissue ultimate strains by ±1 SD from their mean values changed vertebral strength by at most ±8%, an effect that was relatively uniform across all the specimens (**Figure 2-3)**. The relative strengths of the fully ductile (no tissue fracture) and fully brittle (no tissue yielding) cases from the reference case were +11%, and -22%, respectively (**Figure 2-3**).

Overall strength changed similarly for similar (±1 SD) changes in trabecular versus cortical ductility (**Figure 2-3**). Increasing the cortical ultimate strain from the -1 SD value (1.3%) to the +1 SD value (3.1%), with the trabecular ductility held constant, increased vertebral strength by an average of 7%; increasing trabecular ultimate strain from the -1 SD value (5.1%) to the +1 SD value (12.5%), with the cortical ductility held constant, also increased vertebral strength by an average of 7%.

For all cases, only a tiny proportion of tissue failed when the whole bone reached its point of structure-level failure. Across the six specimens, the proportion of yielded tissue was at most 1.3% (**Figure 2-4A**), while the proportion of fractured tissue was at most 0.3% (**Figure 2-4B**); therefore, total proportion of failed tissue was at most 1.6% at the structure-level failure. Of this total 1.6%, the majority of tissue failure occurred by tissue-level yielding rather than fracture (**Figure 2-4C**). Across the six specimens, 81 ± 7% of the total tissue-level failure occurred by yielding, while only 19 ± 7% occurred by fracture.

The failure mode (tension versus compression) and location (trabecular versus cortical) of the failed tissue were relatively insensitive to typical variations in tissue ductility. The ratio of failed tissue in tension to failed tissue in compression was less than one for all the specimens (**Figure 2-5A**), indicating that compressive failure was the dominant mode of failure. However, this ratio was generally higher, indicative of more tensile failure, in specimens having lower BV/TV values. The ratio of failed tissue in the trabecular compartment to failed tissue in the cortical compartment was approximately constant for the different simulation cases, and greater than one for all specimens, indicating that trabecular compartment was the dominant location of failure (**Figure 2-5B**).

2.4. Discussion

The overall goal of this study was to elucidate the effect of typical population-variations in tissue-level ductility on human vertebral strength. We found that compared to the reference case, varying both cortical and trabecular tissue ultimate strains by ±1 SD from their mean values changed

vertebral strength by at most ±8%, a relatively small effect. Further analysis revealed that only a tiny proportion of tissue failed (< 2%) when the whole bone reached its point of structure-level failure (**Figure 2-4**), and that the failure mode (tension versus compression) and location (trabecular versus cortical) of this tiny amount were relatively insensitive to typical variations in tissue ductility (**Figure 2-5**). These findings suggest that it is the overall load transfer within the whole vertebral body —determined by bone volume fraction and microstructure— that dictates where failure occurs rather than the typical variations in the ductility of the tissue. Together these findings suggest that typical variations in tissue ductility might have a relatively modest impact on vertebral strength compared to the multiple-fold variations in vertebral strength that are typically observed across any elderly population.

It should be mentioned that we only have varied the cortical and trabecular tissue ductility by ±1 SD from their mean values, which covers 68% of the total population variations statistically. Although a higher variation in tissue-level ductility would accentuate the corresponding variations in vertebral strength, our simulations of the two extreme cases of tissue-level ductility —fully ductile and fully brittle behavior— show that the variation in vertebral strength is bounded by ~±20%, relative to the reference case, still relatively modest in comparison to the multiple-fold variations in strength that are typically observed across any elderly population.

Our results also suggest that comparable variations —±1 SD from the mean value— in the trabecular or cortical ductility have similar influences on whole-bone strength. Finite element studies have indicated that cortical shell could account for 40–50% of the load sharing under compressive loading [34,59]. This could imply that cortical tissue plays an equal role in vertebral strength as the trabecular tissue, and therefore explain why variations in failure properties of the cortical tissue have a similar impact on overall strength compared to variations in failure properties of the trabecular tissue. However, it should be brought to attention that the ultimate strain value for trabecular or cortical tissue is not well known due to the technical challenges associated with ductility testing of small samples of bone tissue [22], and that these observations are based on the limited data available. Better characterization of the ultimate strain values or differentiation between the tensile and compressive post-yield behavior might change the relative influence of

trabecular and cortical tissue ductility on vertebral strength.

The ability of our computer models to simulate both fracture and yielding of the bone tissue made it feasible to evaluate their relative roles at the microstructural level. Our analyses suggest that majority of the tissue-level failure occurs by yielding whereas only a marginal proportion of the tissue fails by fracture. This finding seems to be consistent with the experimental observations by Fyhrie and colleagues who reported a low incidence of microfracture (tissue-level fracture) of vertically oriented trabeculae in the trabecular bone, even after a substantial mechanical overload [60]. In addition, Yeh and Keaveny, using finite element analysis, made a similar observation and suggested that if the ultimate strain of individual trabeculae was greater than 2% — which was the case in our study — microdamage (tissue-level yielding) rather than microfracture would be the primary mode of damage accumulation in the trabecular bone [61]. These observations for small trabecular bone specimens in addition to our results for whole-bone specimens could suggest that structure-level failure of vertebral trabecular bone may be dominated by tissue-level yielding rather than tissue-level fracture.

Nevertheless, our study has a number of limitations. First, as noted above, the ultimate strain value for trabecular or cortical tissue is not well known due to the technical challenges associated with ductility testing of small samples of bone tissue [22]. Although, changing the ultimate strain values may change the absolute value of our predicted vertebral strength, the results of this study are still insightful as they are based on the relative changes in vertebral strength due to variations in tissue-level ductility rather than the absolute values. Second, ultimate strain value was assumed the same in tension and in compression for both tissue since the available data in literature are for tensile ultimate strain of both trabecular and cortical tissue [19,20]. To differentiate the effect of tensile versus compressive ultimate strain on vertebral strength, a parameter study was conducted on one specimen, which indicated that vertebral strength was dominated by tissue compressive ultimate strain (**Appendix 6.1**). This suggests that more experiments need to be done to better characterize compressive behavior of bone tissue and its changes with aging, disease and treatment. Third, we only have simulated a uniform compression loading of the vertebrae via PMMA. Previous studies using micro-CT-based finite element analysis have shown that the overall load-sharing trends are

relatively insensitive to the presence of a disc [34]. Thus, we would not expect to see a significant change in our results with an intervertebral disc instead of PMMA at the endplates. However, analyzing other loading configurations could be a topic of future work. Last, this study has been performed on six human cadaveric vertebrae. The choice of using six specimens was based on the outcome of a previous study with twelve vertebrae, which concluded that the effect of tissue-level ductility on whole-bone strength is mostly uniform across all specimens of an anatomic site subjected to similar loading and suggested that future theoretical work in this area should not require large sample size [54]. It is also worth mentioning that although the six specimens analyzed in this study were diverse and spanned a wide range in their measured strength, the effect of typical population variations in tissue-level ductility on vertebral strength was uniform across the six specimens.

The findings of this study may have potential clinical implications. Our results indicated that typical population variations in tissue-level ductility only introduced a small uncertainty in vertebral strength. To better elucidate the role of this uncertainty in fracture risk assessment, cadaver testing data on vertebral strength from Mosekilde et al. [62] were plotted along with the error bars representing the uncertainty found in this study (±8% variation in strength with respect to the reference case; **Figure 2-6A, B**). Clinical cut-points representing the vertebral compressive strength below which individuals are at high risk of fracture were also specified for both sexes (dotted lines; Kopperdahl et al., 2014). In the elderly population, the strength values are already well below the clinical cut-points, most probably due to the age-related bone loss. Therefore, the small uncertainty due to variations in tissue ductility may only result in few individuals in this population to go below or above the clinical cut-points, and therefore, may not have a strong influence on fracture risk assessment. Even after increasing the uncertainty by including the two extreme cases of fully ductile and fully brittle (+11% and -22% respectively, with respect to the reference case; **Figure 2-6C, D**), very few individuals in the elderly population cross the clinical cut-points. Unlike the youth and the elderly population that have strength values well above or below the clinical cut-points respectively, vertebral strength values in the middle-aged population are closer to the clinical cut-points. Together these results suggest that typical population variations in tissue-level ductility might play a more important role in fracture risk assessment of the middle-aged population compared to their relatively minor role in the youth and the elderly.

Table 2-1: The combinations of simulated tissue-level ultimate strains. For typical population variations (cases one through nine), the ultimate strain value was assumed the same in tension and compression, but different for trabecular or cortical tissue. For fully ductile, there was no fracture and the tissue could continue to yield infinitely. For fully brittle, there was no yielding and tissue fractured as soon as it reached the yield point.

Case	ε_{ult}^{trab}	$\varepsilon_{ult}^{cort.}$
fully brittle	0.33/0.69 [a]	0.33/0.69 [a]
1	5.1	1.3
2	5.1	2.2
3	5.1	3.1
4	8.8	1.3
5	8.8	2.2
6	8.8	3.1
7	12.5	1.3
8	12.5	2.2
9	12.5	3.1
fully ductile	∞	∞

[a] For the fully brittle case, the ultimate strain was set equal to the yield strain, which was the same for cortical and trabecular tissue, but was different in tension (0.33%) and compression (0.69%).

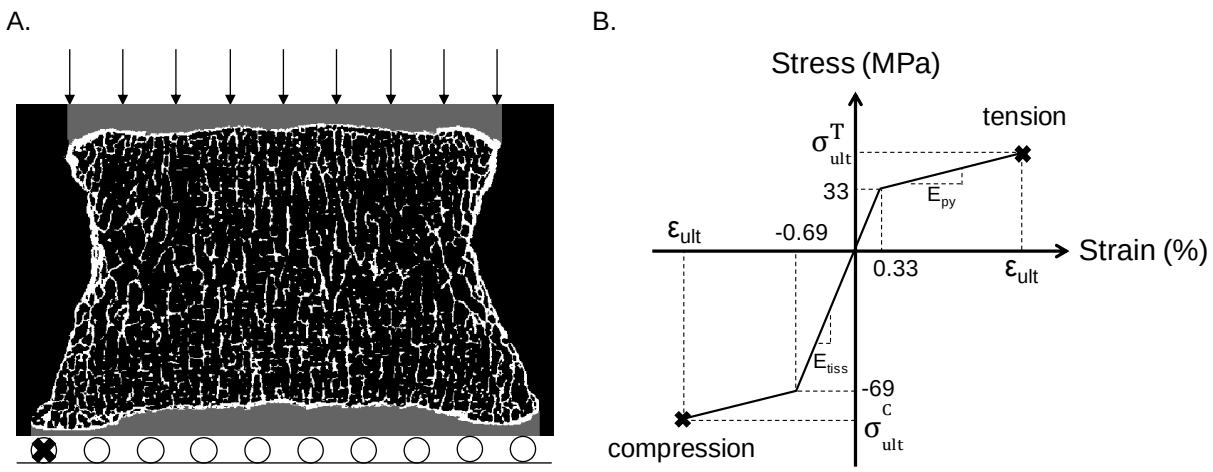

Figure 2-1: A) Boundary conditions used in the finite element analysis to simulate habitual loading. B) Material model depicting the stress–strain response at the tissue-level for both cortical and trabecular tissue. ε_{ult} represents the tissue-level ultimate strain, which was different for the cortical vs. trabecular tissue, but was assumed the same in tension and compression in the main analysis.

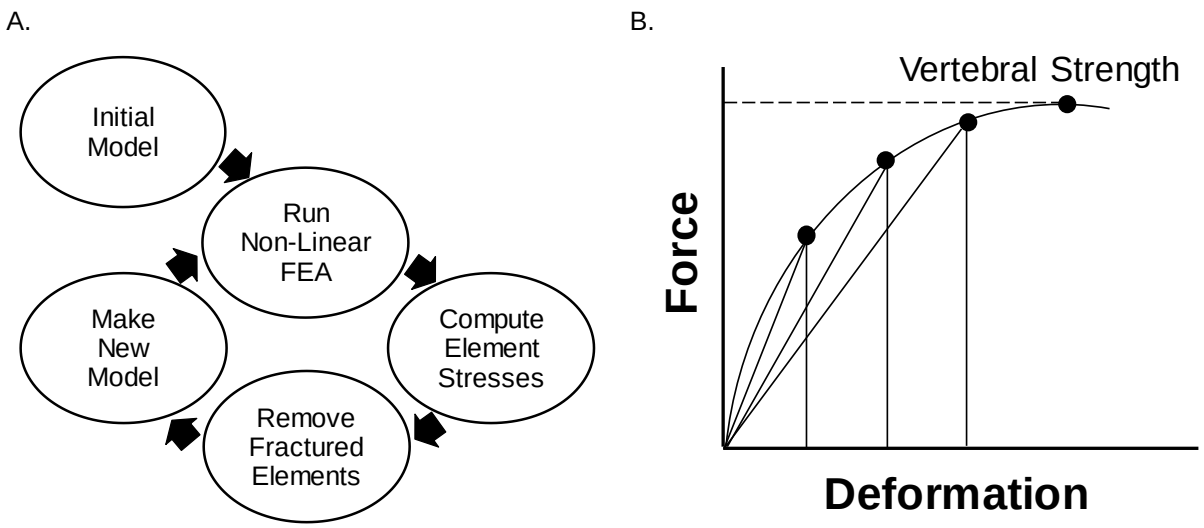

Figure 2-2: A) Flowchart of the iterative approach that included both tissue yielding and tissue fracture, and was performed for each of the incremental displacement steps per simulation case per specimen. B) The overall force-deformation curve; each bullet represents the non-linear analysis results for the corresponding displacement increment.

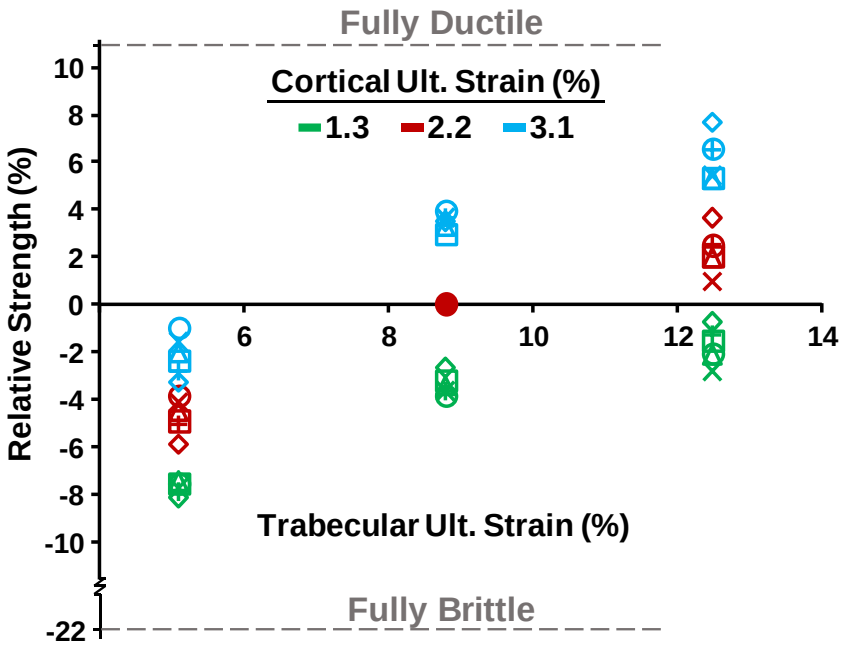

Figure 2-3: Vertebral strength versus ultimate strain of the trabecular tissue, shown for different values of ultimate strain for the cortical tissue; strength is expressed as the percent difference from the specimen-specific reference case. Each marker represents one specimen.

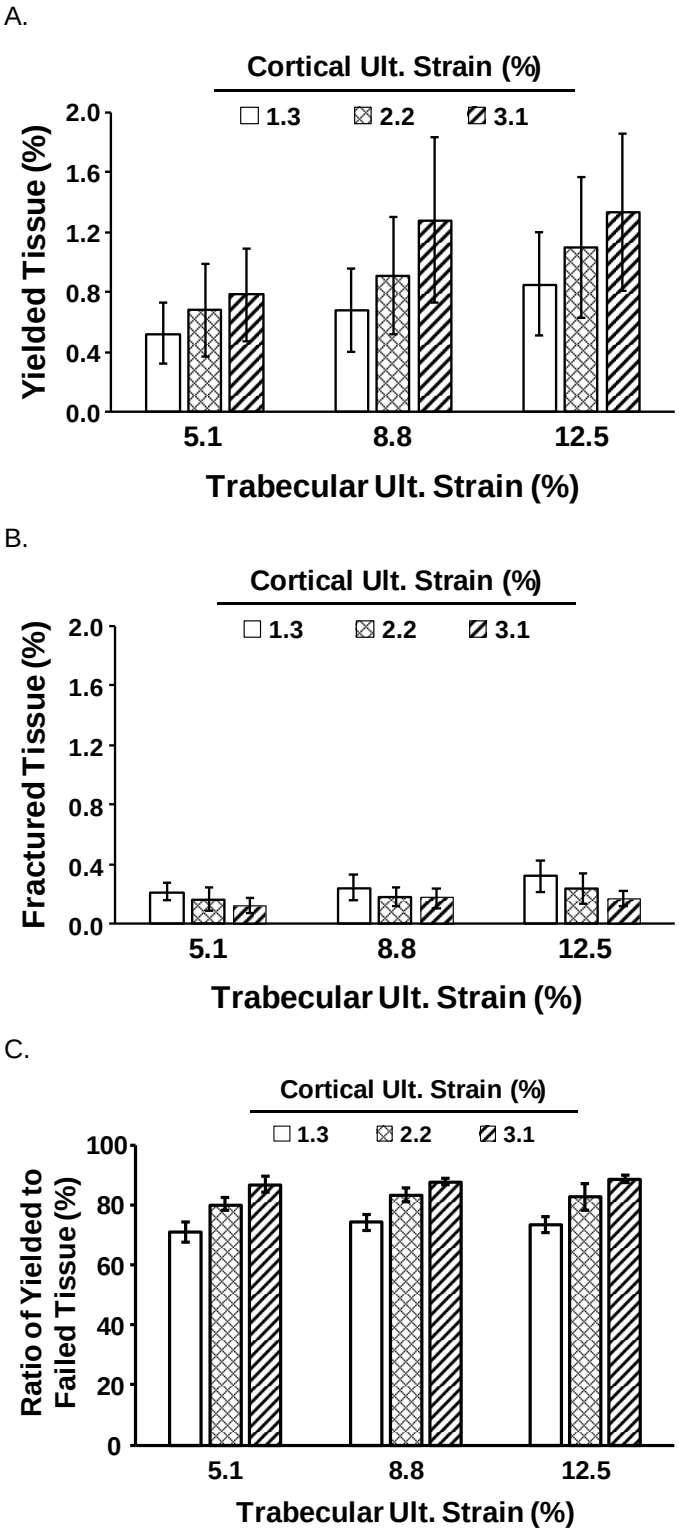

Figure 2-4: Proportion of A) yielded tissue, B) fractured tissue, and C) yielded to failed tissue versus ultimate strain of the trabecular tissue, shown for different values of ultimate strain for the cortical tissue. Error bars represent one standard deviation.

A.

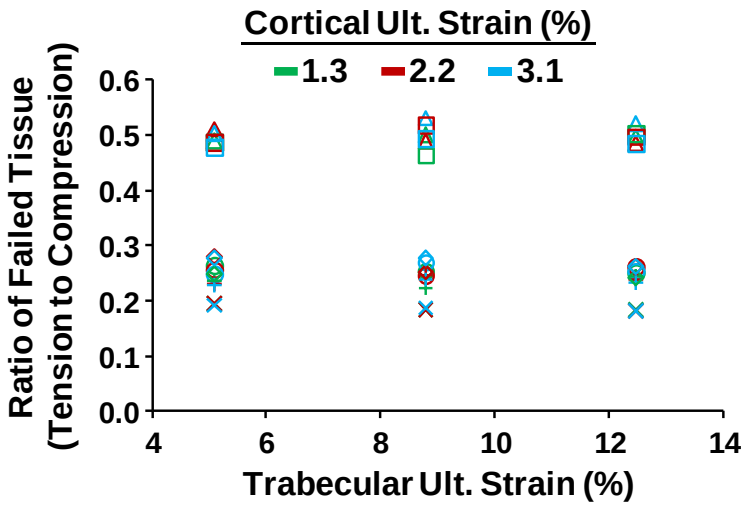

B.

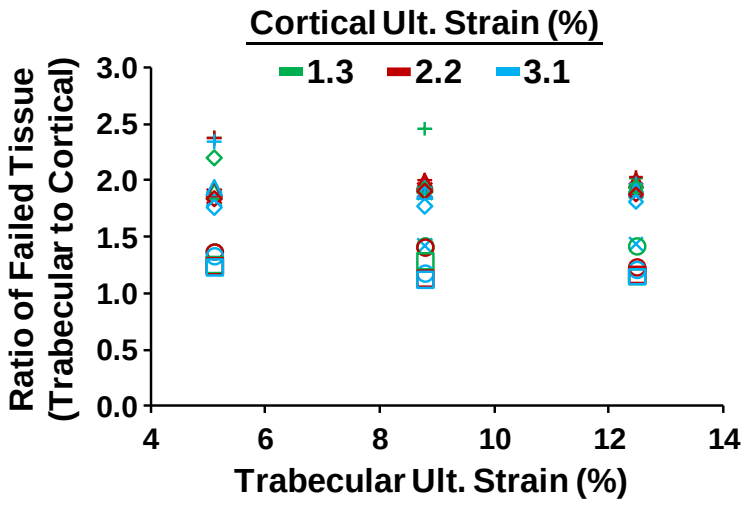

Figure 2-5: Ratio of failed tissue A) in tension to compression B) in trabecular to cortical compartment versus ultimate strain of the trabecular tissue, shown for different values of ultimate strain for the cortical tissue. Each marker represents one specimen.

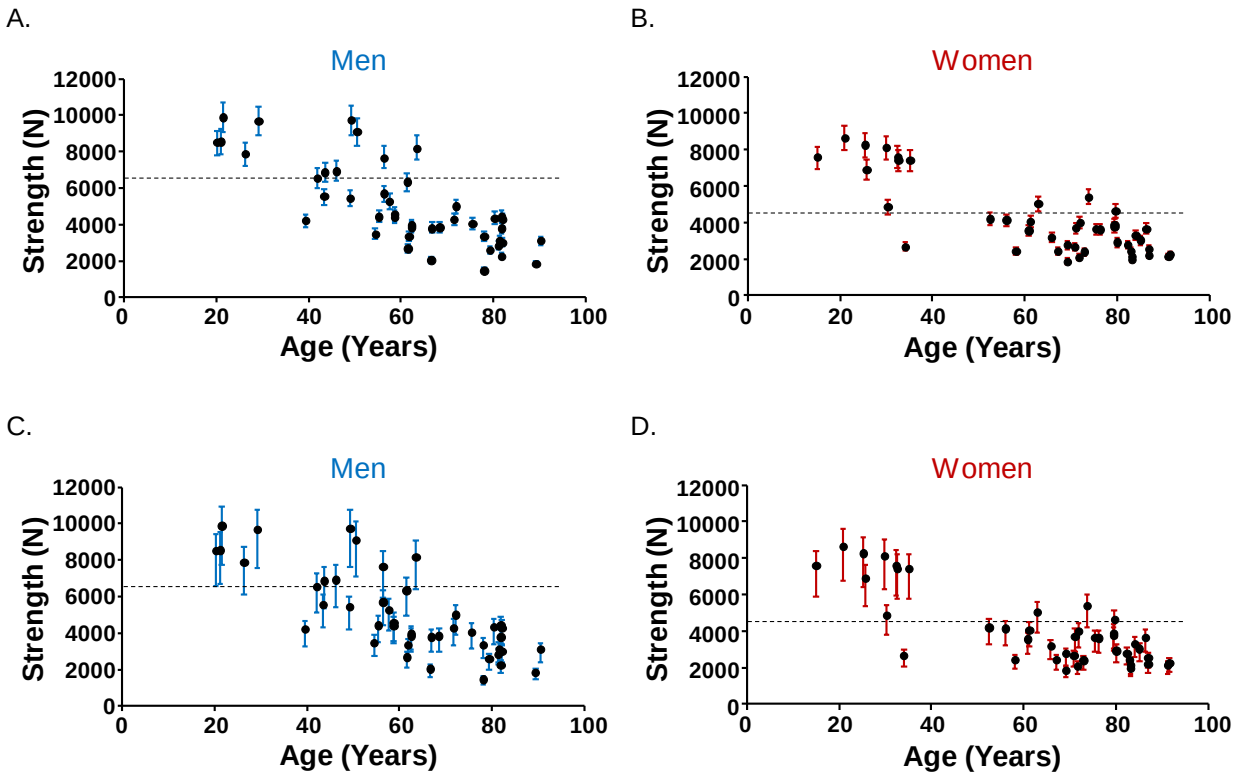

Figure 2-6: Vertebral strength vs. age (data from [62]) plotted along with the error bars that represent the uncertainty found in this study. First row error bars indicate the typical population-variations (±8% with respect to the reference case) in A) men and B) women. Second row error bars indicate the extreme cases variations (+11% for fully ductile and -22% for fully brittle with respect to the reference case) in C) men and D) women. The dotted lines represent the clinical cut-points for vertebral strength [63].

3. Effective tissue modulus of human vertebral trabecular bone

3.1. Introduction

One outstanding issue in bone mechanics concerns tissue modulus of trabecular bone. Characterizing this property and its role in the mechanical behavior of trabecular bone may have potential clinical and scientific importance. Clinically, knowledge of the bone tissue modulus could be used to elucidate the effects of aging, disease, and drug treatment. Scientifically, tissue modulus is a fundamental element of understanding the mechanical behavior of bone, and its characterization is especially important in developing a better mechanistic understanding of bone quality and fracture risk. Furthermore, tissue modulus is required as input for both computational [15,29,35,38,54,64,65] and analytical [18] models, and therefore, represent an important basis for micromechanical analysis of trabecular bone as well as whole-bone specimens.

Although numerous experimental studies have reported trabecular tissue modulus [66–71], there remains substantial unexplained discrepancy. In part, this discrepancy arises from the difficulty of eliminating potentially large compliance effects during experimental testing at the tissue level [22]. An alternative to mechanical testing of individual trabeculae is to use high-resolution micro-CT based finite element analysis combined with specimen-specific experimental data at the whole specimen (apparent) level to calibrate ‘‘effective’’ tissue properties [64]. Nonetheless, there has been discrepancy in such studies as well [29,46,72], potentially due to the compliance effects associated with the mechanical testing protocols at the apparent level [73–76], or the limitations of the computational models in fully capturing tissue elastic mechanical behavior. Aside from this, the correlation between trabecular tissue modulus and trabecular microarchitecture and bone volume fraction (BV/TV) is not fully understood.

Previous combined finite element-experimental studies have mostly used experimental measurements of stiffness at the apparent level to calibrate effective tissue modulus [29,46,64,72].

This is while experimental measurements of strength are less prone to compliance effects during mechanical testing compared to experimental measurements of stiffness and therefore, are expected to provide a more accurate measurement. Furthermore, these studies were performed on small specimens of trabecular bone [29,46,72], although biomechanical testing of whole-bone (larger) specimens is less sensitive to machine compliance effects. In addition, trabecular architecture is preserved intact in whole-bone specimens.

In this context, the goal of this study was to provide further insight into the tissue modulus of trabecular bone and better elucidate its relation with BV/TV and trabecular microarchitecture. We developed a method using a combination of biomechanical testing and non-linear micro-CT-based finite element analysis (FEA) based on strength behavior of whole bone specimens to calibrate effective tissue modulus of trabecular bone. By adding tissue-level ductility as another parameter to our finite element analyses, our computational models were capable of simulating tissue-level fracture as well. Therefore, there were two variables in the finite element models: tissue modulus and tissue ductility. To account for the unknown degree of tissue-level ductility while calibrating effective tissue modulus, a parameter study was performed in which the ductility of cortical and trabecular tissue was varied across a range of typical values. The calibration process was performed for each of the simulated combinations of tissue ductility.

3.2. Materials and Methods

3.2.1. Specimen Preparation and Imaging

Eight L1 human vertebrae (age = 70 ± 15 years, range = 54 – 89 years; 5 female, 3 male) were used in this study. The specimens were micro-CT scanned at the nominal resolution of 37 μm (Scanco Medical AG; Brüttisellen, Switzerland), thresholded, and coarsened to 74 μm voxel size to facilitate computational analysis. The trabecular and cortical compartments were then identified, using a two-dimensional ray-based search algorithm previously developed for the vertebral body ([35], IDL software suite, ITT Visual Information Solutions, Boulder, CO, USA).

3.2.2. Biomechanical Testing

After micro-CT scanning, the specimens were embedded in PMMA on the two ends and were subjected to uniaxial compression test (MTS 810, Eden Prairie, MN) at room temperature, while being kept hydrated. A non-linear force-deformation curve was generated for each specimen, the local maximum of which was defined as the experimental vertebral strength.

3.2.3. Finite Element Analysis (FEA)

Voxel-type finite element models were created for each specimen by converting each voxel into an 8-noded brick element (74 μm element size; [65,77]), and were subjected to uniaxial compressive loading. The material constitutive model, which included kinematic large-deformation geometric non-linearity effects [17], assumed identical tissue-level elastic and yield properties for the cortical and trabecular tissue, but had different tissue-level ultimate strains for each tissue (**Figure 3-1**). To account for the unknown degree of tissue-level ductility, for each specimen, a parameter study was performed in which the ultimate strain value for each of the trabecular and cortical tissue was varied across a range of typical values. All finite elements were assigned the same hard tissue material properties, having an isotropic elastic modulus of 10 GPa, Poisson's ratio of 0.3, and yield strains of 0.69% in compression and 0.33% in tension, respectively [29]. After yielding, the tissue could continue to deform in a plastic manner (the post yield modulus was 5% of the initial elastic modulus, **Figure 3-1**) until its strain exceeded the prescribed ultimate strain, at which point the tissue was assumed to fracture. Assuming the ultimate strain of the bone tissue to be the same in tension and compression, the post-yield plastic properties varied between each parametric model: three values of cortical ultimate strain (2.2 ± 0.9%, McCalden et al., 1993) and three values of trabecular ultimate strain (8.8 ± 3.7%, Hernandez et al., 2005) for a combination of nine cases per specimen. Two extreme cases of fully ductile and fully brittle were also simulated to provide the theoretical bounds (**Table 3-1**).

To simulate tissue-level fracture, an iterative analysis was performed in which the overall displacement was applied incrementally [54]. For each incremental displacement step, a fully non-

linear finite element analysis was performed which could by itself only simulate element-level yielding, but not fracture. However, after each iteration, strains were computed at each element centroid, and once either the maximum or minimum principal strain at any element centroid exceeded the assumed respective tissue-level tensile or compressive ultimate strain, the element was assumed to have fractured and its elastic modulus was reduced 100-fold to produce an updated model. These updated models were then reloaded, from zero load up to the next displacement increment and the entire process was repeated until the full displacement was applied. In this way, an overall non-linear force-deformation curve was generated for the vertebral body that had a local maximum value of applied force, which was defined as the vertebral strength.

For each vertebra, the predicted vertebral strength was then compared against the experimental strength for each of the simulated combinations of tissue ductility. If the percentage difference was less than or equal to 5%, the initial estimate of tissue modulus was recorded as the effective tissue modulus; if not, a new estimate of tissue modulus was obtained by linear scaling and the analysis was repeated until the percentage difference between the computational and experimental strengths was less than or equal to 5%. This scaling resulted in a range of effective tissue modulus values for each specimen, corresponding to the range in assumed degree of tissue-level ductility (**Figure 3-2**).

Models contained 120 million degrees of freedom on average and were solved using a highly scalable, implicit parallel finite-element framework —Olympus (Adams et al. 2003; Adams et al. 2004) running on a Dell Linux Cluster supercomputer (Stampede, Texas Advanced Computing Center). 2300 CPU hours were required per incremental step, per case, per specimen, resulting in a total of 15×10^5 used CPU hours.

3.2.4. Outcomes and Statistical Analysis

As mentioned earlier, the main outcome was a range of effective tissue modulus values for each specimen, corresponding to the range in assumed degree of tissue-level ductility. The mid-range was used as the specimen-specific effective tissue modulus in further analyses. Linear regression

was used to investigate the relation between this specimen-specific effective tissue modulus and trabecular microarchitecture and BV/TV. All statistical tests (JMP 13; SAS Institute, Cary, NC USA) were considered significant at $p < 0.05$.

3.3. Results

The mean (± SD) value of effective tissue modulus for vertebral trabecular bone was 18.5 ± 7.4 GPa, and varied in the range of 10–30 GPa across the eight vertebrae. The range of computed effective tissue modulus within each vertebra (corresponding to the range in assumed degree of tissue-level ductility) was small (within 20% of the mean value for each specimen) compared to the range of the mean values across all the eight vertebrae (up to 3-fold increase from one specimen to another; **Figure 3-3**).

Effective tissue modulus was negatively correlated with BV/TV of each vertebra ($R^2 = 0.51$, $p < 0.05$), but showed no dependence on age ($p > 0.5$) or trabecular microarchitecture ($p > 0.1$) (**Figure 3-4**).

Effective tissue modulus of each vertebra was also negatively correlated with its experimental strength ($R^2 = 0.64$, $p < 0.05$, **Figure 3-5**), indicating that higher values of the computed effective tissue modulus were associated with lower values of directly measured vertebral strength.

3.4. Discussion

The overall goal of this study was to provide further insight into the tissue modulus of trabecular bone and better elucidate its relation with bone volume fraction and trabecular microarchitecture. Our results indicated that effective tissue modulus of vertebral trabecular bone varied greatly among the specimens and was negatively correlated with bone volume fraction of each vertebra ($R^2 = 0.51$, $p < 0.05$). These results suggest that there can be 3X variation in tissue modulus across

the elderly human vertebrae, about 50% of which may be explained by variations in BV/TV. Together these findings suggest that as trabecular bone becomes older and thus more porous due to an imbalance between bone formation and resorption, the tissue may become stiffer to compensate for the bone loss.

The negative correlation between effective tissue modulus and BV/TV may be explained by the slowdown in bone turnover rate or the imbalance in bone remodeling, caused by aging or diseases such as osteoporosis. As trabecular bone becomes older, it becomes more porous due to an imbalance between bone formation and bone resorption. This imbalance is also accompanied by a slowdown in the bone turnover rate, which results in bone tissue becoming older, more mineralized on average and thus stiffer. Therefore, a decrease in overall BV/TV might be accompanied by an increase in trabecular tissue modulus. This hypothesis is supported by a number of studies. For example, Zioupos et al. reported that microhardness (and by implication tissue modulus) increased with decreased BV/TV in human femoral trabecular bone [78]. McNamara et al. observed an increase in the stiffness and strength of ovariectomized rat trabeculae compared to the controls and reported that these increases were associated with a significant increase in the mineral content of these trabeculae, although overall bone mineral density and mass were reduced [79,80]. This would also imply a negative correlation between tissue modulus and BV/TV. Furthermore, it has been reported that increased calcium content and stiffness occur within individual trabeculae from human osteoporotic vertebral bone compared to the non-osteoporotic trabeculae [81], which may as well imply that tissue modulus decreases with increasing BV/TV.

Nevertheless, it could be possible that our estimates of the effective tissue modulus, which account for the uncertainty in tissue-level ductility, are sensitive to numerical modeling parameters although our results may suggest otherwise. The calibrated effective tissue modulus for specimens having similar BV/TV values (~0.16) varied by a factor of two in the range of 10–20 GPa, the lower end of which is consistent with the results of a previous study that used protocols that would minimize compliance effects [29]. This indicates that our modulus values are not scaled in a same manner or by a relatively constant factor compared to previous studies, which would be expected in the case of existence of partial volume effects since all the specimens were analyzed with the

same voxel size. This suggests that our results may be insensitive to the voxel size and partial volume effects. However, further work which is beyond the scope of this study is required to elaborate more.

Our results may help resolve some of the discrepancy in the reported values of the vertebral trabecular tissue modulus. Previous combined finite element-experimental studies on human vertebral trabecular bone have reported lower values of calibrated effective tissue modulus [46,72] compared to this study and the experimental studies that used nanoindentation [69,71]. This discrepancy is mainly due to the presence of the end-artifacts in the mechanical testing protocol of the previous combined finite element-experimental studies [73–75]. Our range for the effective tissue modulus of trabecular bone is mostly consistent with the results of a previous combined finite element-experimental study that used protocols that would minimize end-artifact effects [29] except for the very high values that could be due to the partial volume effects in the current study as discussed previously. Overall, these results suggest that the elastic modulus of trabecular tissue is at the higher end of the range of values reported by the nanoindentation studies and is comparable to that of the cortical tissue.

This study has a number of limitations. First, only eight specimens were utilized in this study. These specimens span a wide range in terms of age, sex and bone volume fraction. Furthermore, we were able to establish statistically significant trends between effective tissue modulus, BV/TV and microarchitectural parameters with our small sample size; thus, repeating the study with a bigger sample size is unlikely to change the conclusions of this study. Second, to decrease the computation costs, region averaging was used to coarsen all the image resolutions to 74 μm although it is recommended that for better numerical convergence, the resolution should be one-fourth of the mean trabecular thickness [82,83]. Therefore, our estimates of the absolute values of the effective tissue modulus might be affected by these partial volume effects, especially because we found very high values for some specimens (E_t > 20 GPa). However, since all the specimens are susceptible to the same partial volume effects in case of existence of any, our conclusions which were mostly concerned with the variations in the effective tissue modulus caused by the

variations in tissue-level ductility, and the trends between effective tissue modulus and microarchitectural parameters are unlikely to change, although the absolute values might change.

The results of this study may have clinical implications. Our results suggest that there can be a large variation in the tissue modulus of human vertebral trabecular bone, due partly to the variations in BV/TV. This suggests that as BV/TV decreases with aging or diseases such as osteoporosis, tissue modulus increases, which can compensate for the overall strength. However, very high tissue modulus values in some individuals may have an overall weakening effect, as hyper-mineralization and very stiff individual trabecula may result in overall embrittlement and therefore, reduced vertebral strength. This suggests that a high clinical bone mineral density measurement —which also reflects tissue mineralization— might be indicative of lower bone volume fraction and weaker bone in the elderly population, an insight that could potentially be important in osteoporosis fracture risk assessment.

Table 3-1: The combinations of simulated tissue-level ultimate strains; For typical population variations (cases one through nine), the ultimate strain value was assumed the same in tension and compression, but different for trabecular or cortical tissue. For fully ductile, there was no fracture and the tissue could continue to yield infinitely. For fully brittle, there was no yielding and tissue fractured as soon as it reached the yield point.

Case	ε_{ult}^{trab}	$\varepsilon_{ult}^{cort.}$
fully brittle	0.33/0.69 [a]	0.33/0.69 [a]
1	5.1	1.3
2	5.1	2.2
3	5.1	3.1
4	8.8	1.3
5	8.8	2.2
6	8.8	3.1
7	12.5	1.3
8	12.5	2.2
9	12.5	3.1
fully ductile	∞	∞

[a] For the fully brittle case, the ultimate strain was set equal to the yield strain, which was the same for cortical and trabecular tissue, but was different in tension (0.33%) and compression (0.69%).

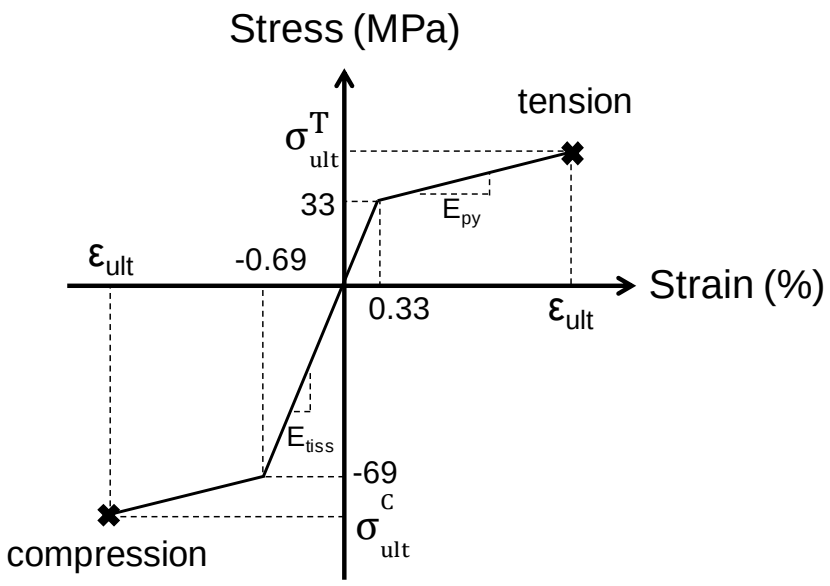

Figure 3-1: Material model depicting the stress–strain response at the tissue-level for both cortical and trabecular tissue. ε_{ult} represents the tissue-level ultimate strain, which was different for the cortical vs. trabecular tissue, but was assumed the same in tension and compression.

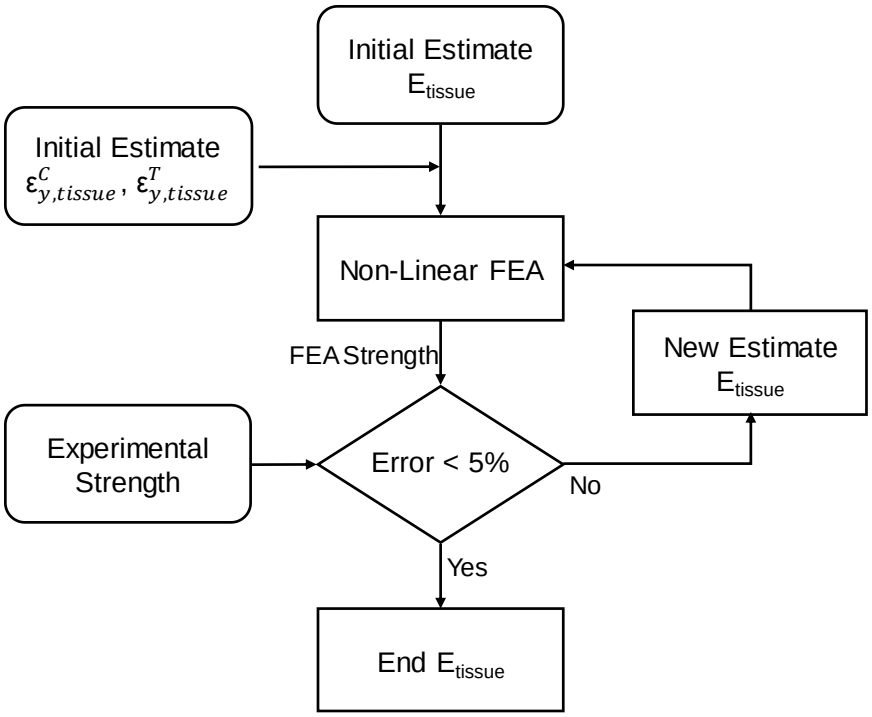

Figure 3-2: Flowchart representing the effective tissue modulus calibration process, performed for every assumed combination of tissue-level ductility (eleven cases in **Table 3-1**).

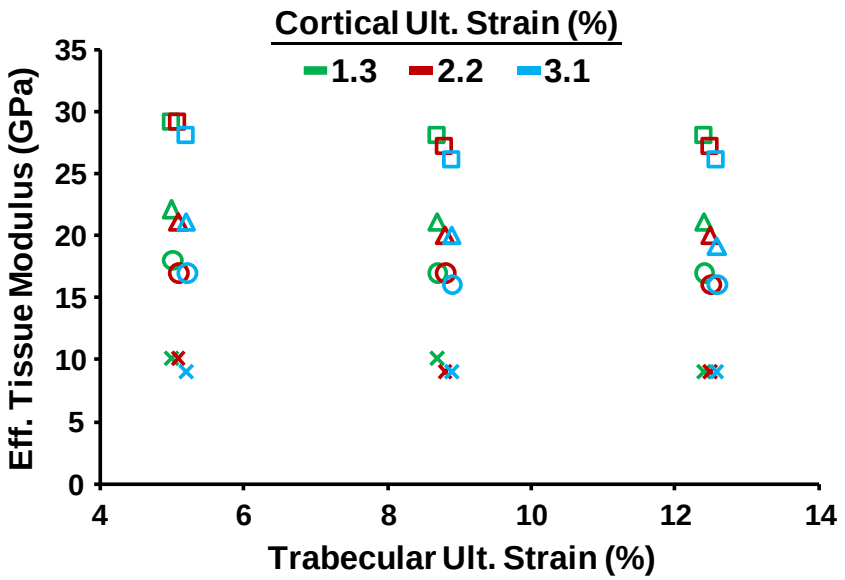

Figure 3-3: Effective tissue modulus vs. trabecular ultimate strain, shown for different values of cortical ultimate strain; each marker represents one specimen. For clarity, data are expanded at each trabecular ultimate strain value and presented for four of the specimens.

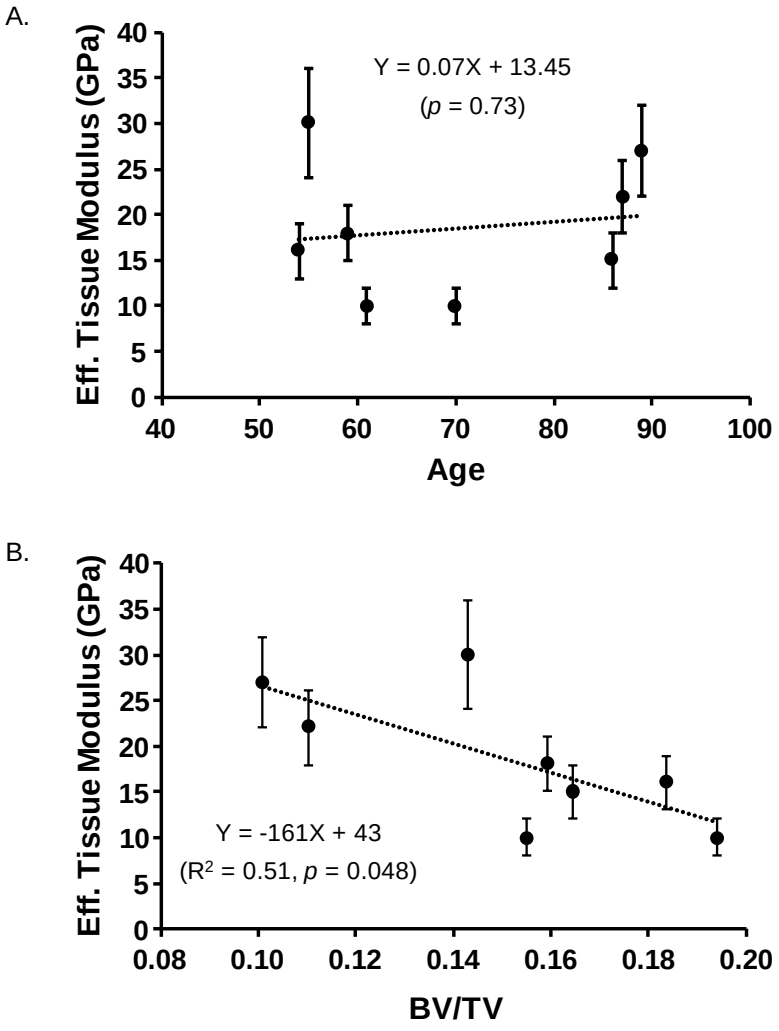

Figure 3-4: Effective tissue modulus versus A) age, and B) bone volume fraction (BV/TV) of each vertebra. Each bullet represents the mid-range for the effective tissue modulus of one specimen; error bars represent the full range for different assumed values of tissue-level ductility.

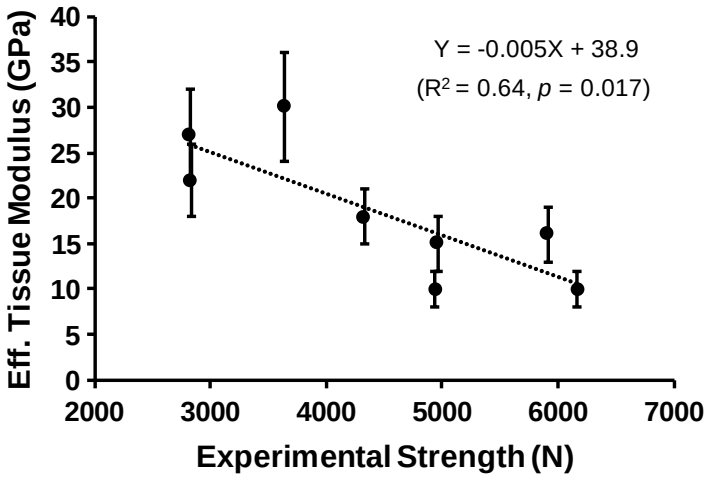

Figure 3-5: Effective tissue modulus versus experimental strength. Each bullet represents the mid-range for the effective tissue modulus of one specimen; error bars represent the full range for different assumed values of tissue-level ductility.

4. Biomechanical Structure–Function Relations for Human Calcaneal Trabecular Bone — Comparison with other Sites

4.1. Introduction

The current clinical standard for diagnosing osteoporosis relies on a measurement of bone mineral density (BMD) by dual energy X-ray absorptiometry (DXA) [84]. However, this modality is under-utilized as most test-eligible patients do not get tested [85]. Such under-utilization encourages seeking alternative diagnostic modalities to DXA. One clinical alternative is quantitative ultrasound (QUS) as applied to the calcaneus, which is widely available, inexpensive, portable, and does not expose patients to ionizing radiation [86–89].

Previous studies on the calcaneus have been primarily focused on two topics: 1) investigating the relation between calcaneal QUS parameters and its bone mineral density [90–92], its microarchitecture [92–96] and its mechanical properties [97–100]; 2) studying its morphometry and age-related changes [97,101–105]. Although from a biomechanics perspective, investigating structure–function relations —the relations between mechanical properties and structure of bone— is key in understanding bone adaptation process, only a few studies so far have explored these relations for human calcaneal trabecular bone [99,106–108]. Furthermore, no study has ever compared the structure–function relations of human calcaneal trabecular bone with other anatomic sites, although these relations can reflect the age-, disease-, or treatment-related bone adaptation process, and therefore, might provide insight into the assessment of calcaneal trabecular bone for diagnosing osteoporosis. Thus, it remains unclear how well calcaneal trabecular bone reflects the general mechanical behavior of the trabecular bone at other anatomic sites.

In this context, the goal of this study was to investigate the biomechanical structure–function relations for human calcaneal trabecular bone and compare these relations to those for trabecular bone from other anatomic sites, including the hip and spine, the major sites of osteoporotic fracture.

For that, the relation between bone volume fraction (amount of bone, the simplest measure of structure) and on-axis yield stress (the simplest measure of function and failure), which constitutes the main structure–function relation, was characterized through a power law model as suggested by Currey [109]. To eliminate the variability of tissue material properties across different sites, finite element analysis with uniform tissue material properties was performed so that the main structure–function relation for calcaneal trabecular bone could be characterized only from its trabecular microarchitecture standpoint, which would not have been possible within an experimental setting. One novel feature of this study lay in normalizing the data, both the bone volume fraction and yield stress, for each anatomic site in order to get insight into how deviations from the mean bone mass for a given site translate to deviations in strength, an insight that could potentially be helpful in eventual fracture risk assessment.

4.2. Materials and Methods

4.2.1. Specimen Preparation and Imaging

For the calcaneus, 25 cylindrical (8 mm diameter, 15 mm length) specimens of trabecular bone from human cadavers (age and sex unknown) were machined such that the specimen's long axis was aligned with the primary trabecular orientation ("on-axis" loading, **Figure 4-1**). The specimens were scanned at an isotropic voxel size of 10 μm using micro-CT (Scanco μCT 100, Scanco Medical, Brüttisellen, Switzerland), from which various microarchitecture parameters were measured (**Table 4-1**). The images were then thresholded and coarsened to 20 μm. Specimens for the other anatomic sites, were used from previous studies [17,110]. As reported elsewhere, 53 cylindrical (8 mm diameter, 20 mm length), cadaveric specimens of trabecular bone from human femoral neck (n=21), greater trochanter (n=7), proximal tibia (n=6), and vertebral body (n=19) were prepared such that the specimen's long axis was aligned with the main trabecular orientation (**Figure 4-1**, [110]). Three-dimensional high-resolution images were obtained for each specimen using micro-CT (Scanco μCT 20, Scanco Medical AG, Brüttisellen, Switzerland) or serial milling. Images were then coarsened using region-averaging to either 40 or 60 μm spatial resolution and thresholded such that the volume fraction matched the experimentally measured value [17].

4.2.2. Finite Element Analysis (FEA)

Voxel-type finite element models were created for each specimen by converting each voxel into an 8-noded brick element [38]. The material constitutive model, which included material and geometric non-linearity effects [17], was a rate-independent elasto-plasticity model [111] and assumed the same hard tissue material properties for each voxel: an isotropic elastic modulus of 16.1 GPa (this value was obtained after calibrating FEA estimates with the biomechanical testing measurements; **Appendix 6.2**), a Poisson's ratio of 0.3, and yield strains of 0.69% in compression and 0.33% in tension for the calcaneal specimens [29] and 0.81% in compression and 0.33% in tension for the other anatomic sites [17]. Displacement-type boundary conditions were used to apply compressive strain. Models contained 3–21 million elements and were solved using a highly scalable, implicit parallel finite-element framework —Olympus [50,52], running on Dell Linux Cluster supercomputers (Stampede2, Texas Advanced Computing Center; Dell, Round Rock, Texas), requiring a total of 31×10^3 CPU hours. For each specimen, a non-linear apparent stress–strain curve was generated, from which the apparent-level yield stress was computed by the 0.2% offset method. These FEA-estimated yield stresses were validated against the experimental measurements for a subset of the specimens (pooled $R^2 = 0.97$, **Appendix 6.2**).

4.2.3. Outcomes and Statistical Analysis

The main outcome was the apparent-level yield stress, as computed by the finite element analysis. A general linear regression model that had this yield stress as the dependent variable and allowed for interaction effects between bone volume fraction (BV/TV) and anatomic site was constructed using log transformations of the data (**Equation 1**). Using this model, the relation between yield stress and BV/TV was compared across different anatomic sites via an analysis of covariance (ANCOVA) with BV/TV as the covariate, followed by Dunnett's *post-hoc* test with the calcaneus as the reference.

$$\sigma_y = a\,(BV/TV)^b;\ \log(\sigma_y) = \log(a) + b \times log\,(BV/TV) \qquad (1)$$

A similar model that did not use log transformations of the data was also investigated; however, analyzing the residuals for both regression models indicated that with the log transformation, the residuals were numerically lower and more randomly distributed.

An alternative comparison of the structure–function relation across sites was investigated whereby both the yield stress and BV/TV were normalized (divided) by their site-specific mean values prior to regression analysis. Using log transformations of these normalized data, general linear regression model was used to compare the normalized yield stress-normalized bone volume fraction relation across different anatomic sites. All statistical analyses were performed in JMP (Version 13.0, SAS Institute Inc.) and were considered significant at $p < 0.05$.

4.3. Results

The mean (± SD) value of BV/TV, apparent modulus, and yield stress for the calcaneal trabecular bone were 0.11 ± 0.03, 722 ± 458 (MPa), and 3.7 ± 2.5 (MPa), respectively. Analysis of variance (ANOVA) followed by Dunnett's *post-hoc* test indicated that for BV/TV, the only site significantly different from the calcaneus was the femoral neck ($p < 0.0001$, **Figure 4-2A**). However, for both apparent modulus and yield stress, calcaneus was most similar to the proximal tibia ($p > 0.5$) and greater trochanter ($p > 0.5$), was significantly lower than the femoral neck ($p < 0.0001$), and trended higher than the vertebral body ($p = 0.07$, $p = 0.23$, respectively) (**Figure 4-2B, C**).

The yield stress–BV/TV power law relation for the calcaneus was most similar to that for the proximal tibia (**Figure 4-3A**). Statistically, no difference was found in the exponents across sites ($p > 0.5$, **Figure 4-4A**); however, the leading coefficient for the calcaneus was different than for the vertebral body ($p < 0.0001$), the femoral neck ($p < 0.005$), and the greater trochanter ($p < 0.05$) (**Figure 4-4B**).

For the normalized results, the structure–function relation did not depend on anatomic site ($p > 0.5$; **Figure 4-3B**). In addition, the normalized yield stress was highly correlated with the normalized BV/TV ($R^2 = 0.85$, $p < 0.0001$).

4.4. Discussion

The results of this study indicate that the relation between yield stress and bone volume fraction of the calcaneus is most similar to that of the proximal tibia. Furthermore, our results demonstrate that while there is no universal yield stress–BV/TV relation for trabecular bone across different anatomic sites for on-axis loading, the general (normalized) yield stress–BV/TV relation is similar for all sites. This similarity in the normalized relation suggests that a given percentage deviation from the mean bone mass has the same mechanical consequence at the calcaneus as it does at the other anatomic sites.

A number of aspects of this study support the validity of our results. All specimens were machined to align the long axis with the main trabecular orientation ("on-axis" loading), so that trabecular anisotropy would not play a role in the observed similarities and differences across different anatomic sites. This enabled characterizing the site-specific architecture effects rather than off-axis properties. Performing finite element analysis so that tissue modulus could be uniform in all the analyses, enabled eliminating its variability across different sites, so that the structure–function relation of interest could be characterized and compared across sites regardless of potential site-specific variations in tissue material properties. Analyzing data from multiple anatomic sites — including the hip and spine, major sites of osteoporosis assessment— made it possible to investigate the structural and mechanical similarities and differences across different anatomic sites and therefore, gain insight into the use of the calcaneus as a site for osteoporosis assessment by any modality.

As the first study to report on the main structure–function relation for human calcaneal trabecular bone and their comparison with other anatomic sites, this study provides new insight into calcaneal trabecular bone, which is the basis of clinical QUS measurements. Our results indicate that

statistically, BV/TV, apparent modulus and yield stress are similar between the calcaneal trabecular bone and all the other anatomic sites analyzed in this study except the femoral neck (**Figure 4-2**). The latter difference might be due to the differences in trabecular architecture, as femoral neck trabecular bone is more plate-like structure than rod-like compared to the other anatomic sites (SMI = 0.42 ± 0.67, **Table 4-1**). In the context of the structure–function relations, no difference was detected in the exponent of the power law relation between yield stress and BV/TV across different sites, whereas the leading coefficients were statistically different. The exponent has primarily been interpreted as an indicator of the failure mechanisms within the trabecular structure according to the cellular solid theory [18,112]. The small range for the exponents of different anatomic sites could therefore suggest that the underlying failure mechanisms might be similar across all sites.

This study has a number of limitations. First, since the specimens were from different cadavers, we did not have paired measurements across sites; therefore, we could not test whether different anatomic sites would have the same age- or osteoporosis-related changes or more specifically, whether a change in the calcaneal bone volume fraction would correspond to the same amount of change in the bone volume fraction of other sites. However, previous studies have reported a correlation between calcaneal BMD (therefore BV/TV) and hip and spine BMD (therefore BV/TV) [113,114], which could suggest that relative variations within the calcaneus bone volume fraction might mimic relative variations in the bone volume fraction of the hip and spine, the major sites of osteoporotic fracture. Second, the data for the structure–function relation were acquired from finite element analysis. Although it is desirable to validate all the results by biomechanical testing, experimental data for a subset of the specimens used in this study, indicated a high correlation with the finite element analysis data (**Appendix 6.2**), validating our FEA methodology. Therefore, we expect that experimental data would lead to the same conclusions. Third, we have assumed a uniform tissue modulus across all anatomic sites, which enabled eliminating its variability across sites. This may introduce a limitation as tissue modulus might vary across sites. However, our data suggest that this is not a major limitation since biomechanical testing measurements of yield stress —which include the tissue modulus effects— are highly correlated with our FEA-estimated yield stresses for each anatomic site (**Appendix 6.2**); thus, we would not expect including site-specific tissue modulus to change our conclusions. Fourth, we only had

access to a small sample size ($n \leq 7$) for two of the sites, which could be the reason why no difference was found in the power law exponents across sites. However, a previous study with a larger sample size for the proximal tibia and greater trochanter did not find any differences in the power law exponents of the yield stress–apparent density (or BV/TV) relation either [110]. Thus, we do not expect our conclusions to change upon increasing the sample size. Last, we have only performed uniaxial on-axis loading, which was sufficient for the goal of this study since it provided across-sites comparisons that were only a function of different architectures rather than off-axis properties; investigating structure–function relations across different anatomic sites for multi-axial loading configurations could be a topic of future work.

The results of this study may have clinical significance in terms of the use of calcaneal trabecular bone in osteoporosis assessment. These results describe an important biomechanical structure–function relation for human calcaneal trabecular bone and demonstrate its similarity with other major anatomic sites. Clinically, this similarity aids in interpreting calcaneal measurements (e.g. made by ultrasound) in assessing risk of osteoporotic fractures. For example, as calcaneal ultrasound parameters are correlated with its bone volume fraction [98], our results indicate that ultrasound estimates of calcaneal bone volume fraction relate to calcaneal bone strength in a similar way as bone volume fraction relates to strength at major osteoporosis sites. Thus, relative variations in ultrasound parameters across individuals may also reflect relative variations in the mechanical properties across individuals — and in a similar fashion as with the hip and spine, key sites for osteoporosis assessment.

Table 4-1: Trabecular microarchitectural information by anatomic site.

Anatomic Site	BV/TV	Conn.D	SMI	Tb.N	Tb.Th	Tb.Sp	DA
FN	0.25 ± 0.06	6.83 ± 2.30	0.42 ± 0.67	1.53 ± 0.17	0.19 ± 0.03	0.64 ± 0.08	1.97 ± 0.23
GT	0.11 ± 0.02	2.97 ± 0.90	1.38 ± 0.20	1.07 ± 0.12	0.14 ± 0.01	0.90 ± 0.10	1.83 ± 0.23
PT	0.12 ± 0.03	3.41 ± 0.91	1.27 ± 0.48	1.18 ± 0.15	0.14 ± 0.01	0.80 ± 0.10	2.25 ± 0.40
VB	0.10 ± 0.04	3.56 ± 1.55	1.85 ± 0.46	1.06 ± 0.17	0.13 + 0.02	0.93 ± 0.15	1.46 ± 0.13
CA	0.11 ± 0.03	4.10 ± 1.72	1.20 ± 0.48	1.16 ± 0.21	0.13 ± 0.02	0.84 ± 0.17	1.98 ± 0.33

BV/TV: Bone Volume Fraction.
Conn.D: Connectivity Density.
SMI: Structure Model Index.
Tb.N: Trabecular Number.
Tb.Th: Trabecular Thickness.
Tb.Sp: Trabecular Separation.
DA: Degree of Anisotropy.

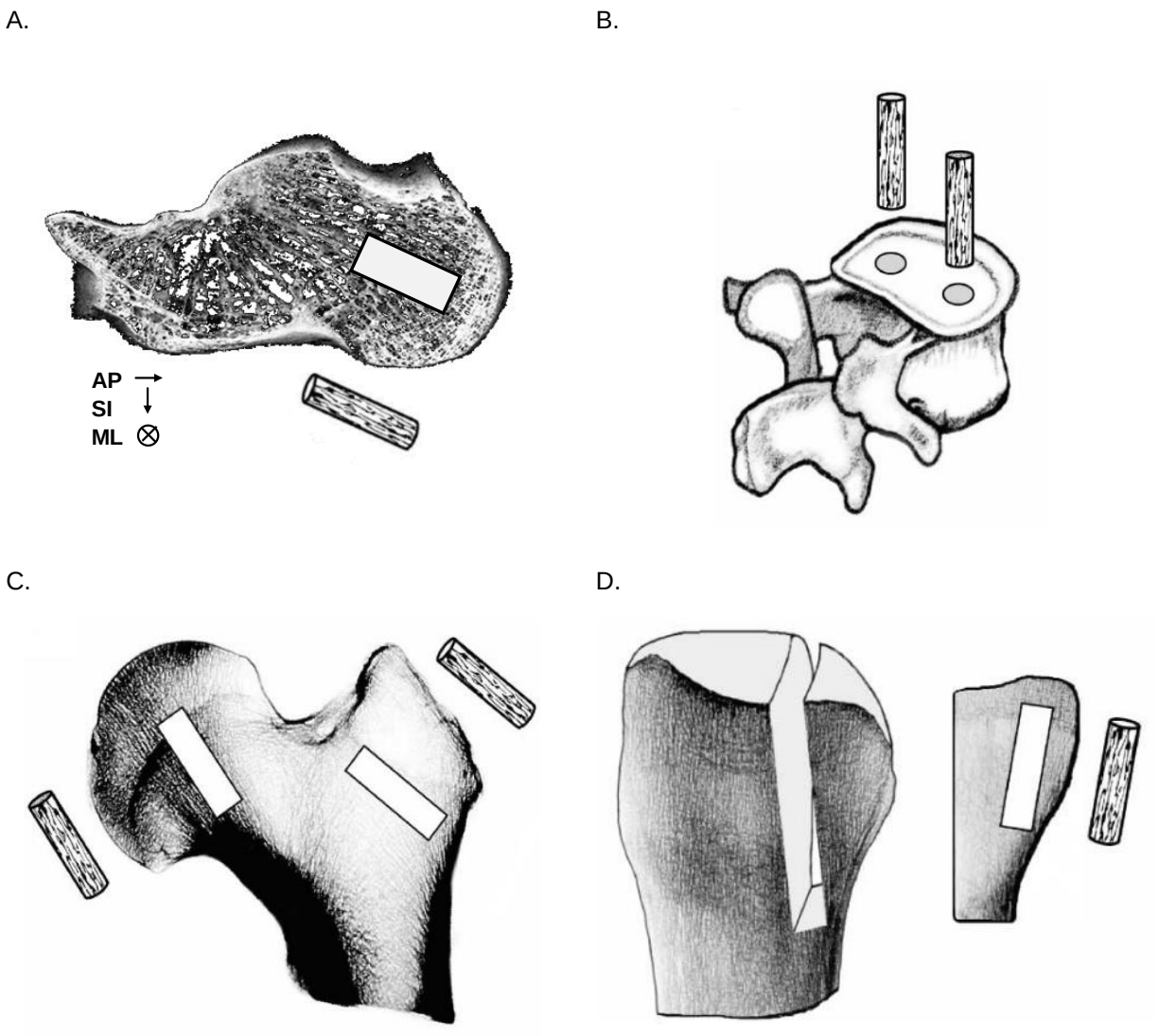

Figure 4-1: On-axis specimens: Specimens were machined such that the longitudinal axis of each core was aligned with the main trabecular orientation. A) Calcaneus. B) Vertebral body. C) Femoral neck and trochanter. D) Proximal tibia (B-D taken from [110]).

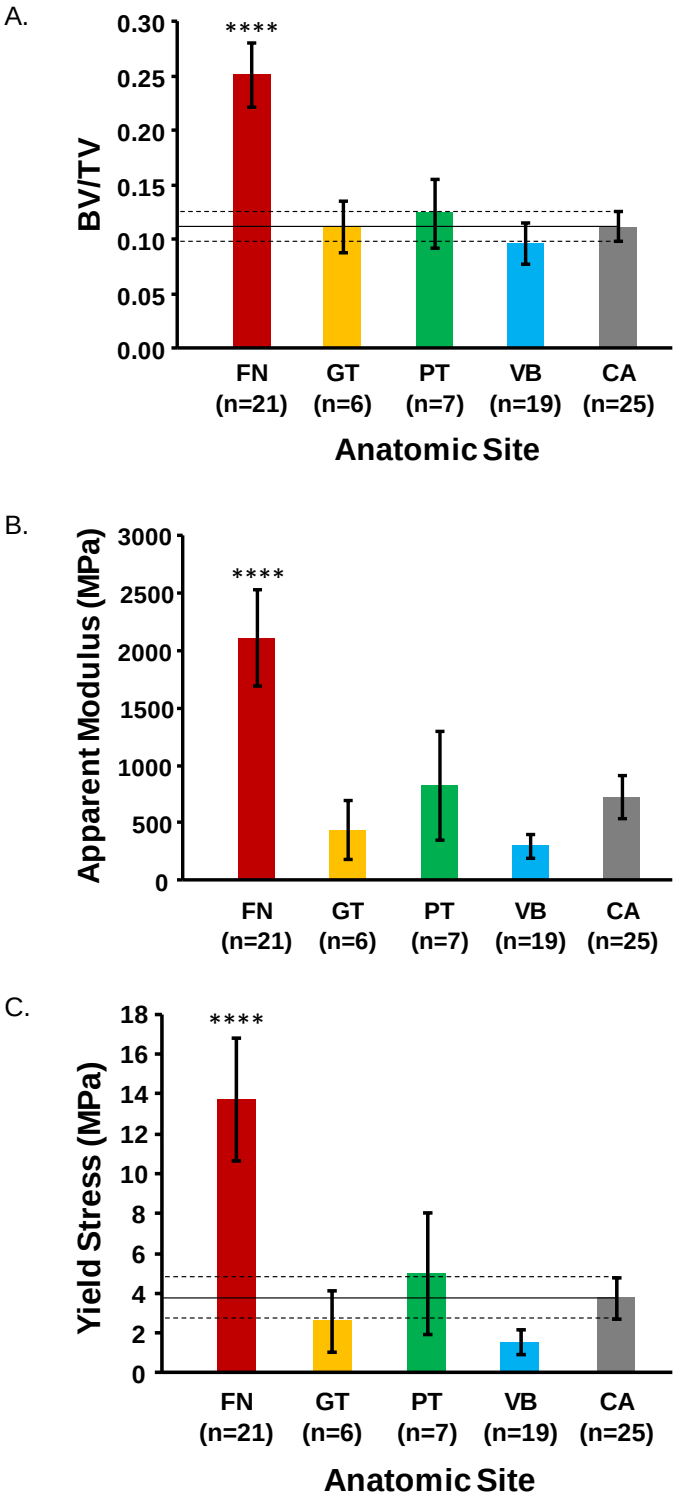

Figure 4-2: A) Bone volume fraction, B) apparent modulus, and C) yield stress, shown for different anatomic sites (FN: Femoral Neck; GT: Greater Trochanter; PT: Proximal Tibia; VB: Vertebral Body; CA: Calcaneus); n represents sample size. Error bars represent 95% confidence intervals. **** $p < 0.0001$, using Dunnett's *post-hoc* test, with CA as the reference.

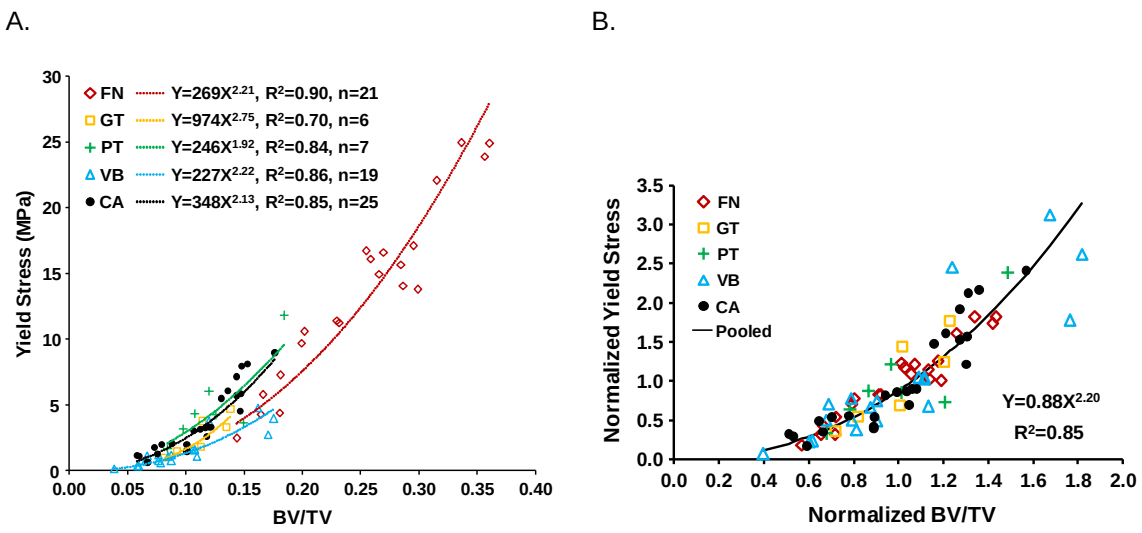

Figure 4-3: Yield stress versus BV/TV for trabecular bone from various anatomic sites (FN: Femoral Neck; GT: Greater Trochanter; PT: Proximal Tibia; VB: Vertebral Body; CA: Calcaneus). A) Unnormalized data; B) Data normalized by their site-specific mean values.

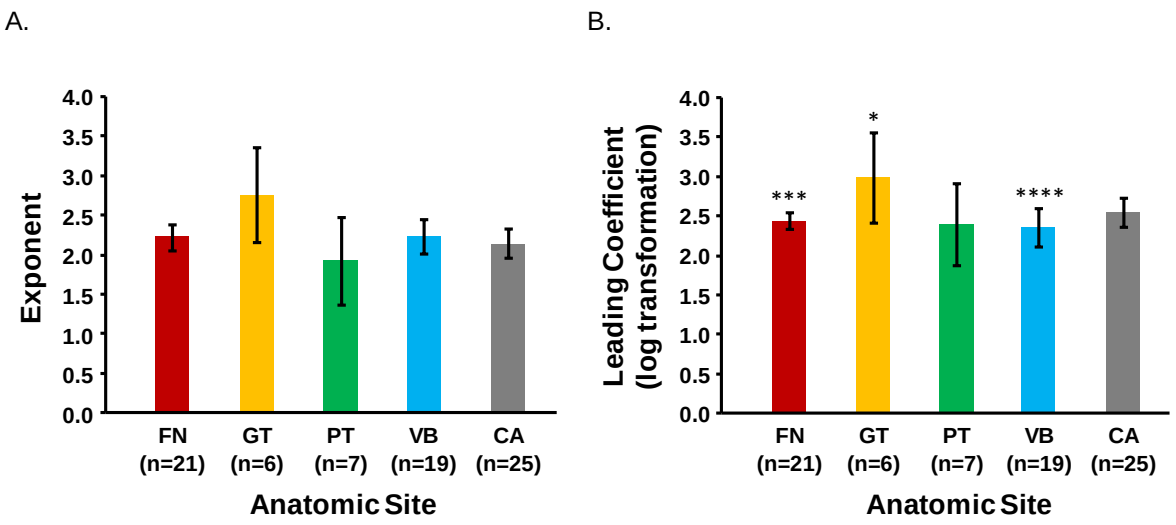

Figure 4-4: A) Exponent and B) Log transformation of the leading coefficient of the power law model for yield stress–bone volume fraction relation, shown for different anatomic sites (FN: Femoral Neck; GT: Greater Trochanter; PT: Proximal Tibia; VB: Vertebral Body; CA: Calcaneus); n represents sample size. Error bars represent standard errors. **** $p < 0.0001$, *** $p < 0.005$, * $p < 0.05$ using Dunnett's *post-hoc* test, with CA as the reference.

5. Conclusions and Future Work

The overall goal of this dissertation was to enhance the current understanding of the biomechanical mechanisms of bone strength and the etiology of osteoporotic fractures. The findings of this dissertation are both scientifically and clinically significant. From a basic science perspective, substantial insight was gained into the tissue material properties, their role on whole-bone strength and the underlying mechanisms by which tissue material properties influence whole-bone strength. From a clinical perspective, the results of this dissertation have provided insight into the bone quality behavior and the quality factors that play a more important role in bone strength. Furthermore, this dissertation has provided insight into the potential use of diagnostic modalities other than the current clinical standard for osteoporosis assessment.

Chapter two explored the effect of tissue-level ductility —a bone quality factor— on vertebral strength. Using high-resolution nonlinear micro-CT based finite element analysis made it possible to conduct a controlled parameter study in which the ultimate strain values of the trabecular and cortical tissue were separately varied, so their individual roles in vertebral strength could be elucidated. Studying the failure mechanisms made it possible to quantify the amount of failed tissue at structure-level failure for each specimen in addition to the location (trabecular vs. cortical) and mode (tension vs. compression) of failure. Our results indicated that varying tissue-level ductility had a relatively modest impact on vertebral strength compared to the multiple-fold variations in vertebral strength that are typically observed across any elderly population. Further analysis revealed that only a tiny amount of tissue failed when the whole-bone failed at the structure level. The location and mode of the failed tissue were mostly uniform across all the different combinations of simulated ultimate strain values. Together these results suggest that it is the overall load transfer within the whole vertebral body that dictates where failure occurs rather than typical variations in the ductility of the tissue. This might explain why varying tissue ductility only introduces a small uncertainty in vertebral strength, an uncertainty that may play a more important role in fracture risk assessment of the middle-aged population compared to a relatively more minor role in fracture risk assessment of the youth or the elderly population.

The main study design in chapter two assumed the same ultimate strain value in tension and compression for both trabecular and cortical tissue since the available data in literature for both tissues are based on tensile biomechanical testing. However, this assumption may not be valid, especially for cortical tissue. Stress–strain curves of cortical bone indicate that cortical tissue is more brittle in compression [58]. In this context, to separate the effect of tensile versus compressive post-yield behavior on vertebral strength, a parameter study was performed in which only one of the four ultimate strain values —cortical/trabecular; tensile/compressive— was varied at a time. Our results indicated that vertebral strength was dominated by the compressive behavior. Although previous studies have mostly focused on tensile brittleness, the results of our study suggest that compressive post-yield behavior plays a greater role in vertebral strength. These results provide new insight into bone quality behavior and suggest that more experiments need to be done in order to better characterize the post-yield behavior of the bone tissue, focusing on the compressive behavior.

Chapter three reported on how analysis of the strength behavior of large bone specimens can be used to estimate the effective modulus of trabecular tissue. In a novel approach that accounted for the unknown degree of tissue-level ductility, this chapter combined experimental and computational techniques to calibrate effective tissue modulus of vertebral trabecular bone. Our results indicated that elastic modulus of the trabecular tissue varied greatly among the specimens and was at the higher end of the range of values reported by the nanoindentation studies [69,71] and was comparable to that of the cortical tissue. Our results also indicated that effective tissue modulus of vertebral trabecular bone was negatively correlated with bone volume fraction of each vertebra. This negative correlation suggests that as trabecular bone becomes older and thus more porous due to an imbalance between bone formation and resorption, the tissue may become stiffer to compensate for the bone loss. However, very high tissue modulus values in some individuals may have an overall weakening effect, as hyper-mineralization and very stiff individual trabecula may result in overall embrittlement and therefore, reduced vertebral strength. This suggests that a high clinical bone mineral density measurement —which also reflects tissue mineralization— might be indicative of lower bone volume fraction and weaker bone in the elderly population, an insight that could potentially be important in osteoporosis fracture risk assessment.

Chapter four investigated the main structure–function relation —relations between mechanical properties and structure— for calcaneal trabecular bone and compared it to that of other anatomic sites. The study utilized a power law model to investigate the relation between yield stress (a measure of bone strength, the most important mechanical property) and bone volume fraction (the amount of bone, the simplest measure of structure). Our results indicated that the relation between yield stress and bone volume fraction of the calcaneus was most similar to the proximal tibia. Statistically, no difference was found in the power law exponents across sites; however, the leading coefficient of the calcaneus was different than the vertebral body, the femoral neck, and the greater trochanter. Despite these differences, the general (normalized) structure–function relations did not depend on anatomic site. This similarity in normalized results may have clinical significance in terms of the use of calcaneal quantitative ultrasound in osteoporosis assessment as it suggests that relative variations in bone volume fraction of the calcaneus relate to the relative variations in its strength the same way as in the hip and spine, the major sites of osteoporotic fractures.

The research presented in this dissertation has several strengths. First, use of high resolution nonlinear micro-CT based finite element analysis made it possible to conduct detailed and controlled parameter studies in order to better characterize bone quality behavior and gain insight into the failure mechanisms by which bone quality factors influence whole-bone strength. Second, combining high resolution micro-CT based finite element modeling with biomechanical testing techniques for whole-bone specimens enabled us to exploit the unique capabilities of each technique and gain insight into the effective tissue properties of vertebral trabecular bone. Third, analyzing multiple vertebrae exhibiting a wide range of bone morphologies made it possible to account for biological heterogeneity and therefore, provide a reasonable degree of external validity to the results. Last, incorporating the latest advances in efficient solver algorithms [50,52] and state-of-the-art supercomputing technology enabled us to perform materially and geometrically nonlinear analysis of whole vertebrae (up to few hundred million degrees of freedom), which may place this research at the forefront of current efforts in computational bone mechanics.

There are two potential areas of future research that can further extend the relevance of the work presented in this dissertation. The first area is associated with nonlinear finite element modeling

of whole bones. Currently, there is no objective way of thresholding the micro-CT images of whole bones. Since subtle differences in thresholding can result in substantial errors in micro-CT-derived mechanical properties [29], changes in the current modeling approach related to thresholding are recommended to improve the accuracy of finite element modeling predictions. In addition, the current findings of this dissertation are limited to uniform compressive loading. Since many osteoporotic vertebral fractures are anterior wedge fractures [115], the response to combined compression and anterior bending is of clinical interest and could be a topic of future work. The second area of future research is motivated by the tissue ductility study that investigated the effect of tensile versus compressive tissue ultimate strain on vertebral strength and found that vertebral strength was dominated by the compressive post-yield behavior of the tissue (**Appendix 6.1**). Although previous studies have mostly investigated tensile brittleness and have measured the tensile ultimate strain value for both trabecular and cortical tissue [19–21], this study suggests that compressive post-yield behavior of the tissue might play a more important role in whole-bone strength and that more experiments need to be done to better characterize the tissue compressive post-yield behavior.

In closure, this dissertation provided insight into the micromechanics of human bone, especially the role of architecture and tissue material properties on whole-bone strength. The first study on tissue material properties (chapter two) provided insight into the effect of tissue ductility on whole-bone strength and whether taking this effect into account could potentially be important in fracture risk assessment. The second study on tissue material properties (chapter three) combined experimental and computational techniques and provided insight into the effective tissue modulus of vertebral trabecular bone and its correlation with age, bone volume fraction and trabecular microarchitecture. The study on architecture (chapter four) provided insight into how structure–function relations in one anatomic site compare to other sites and whether based on this comparison, one site can be used in fracture risk assessment of other sites. Together this dissertation sought to find answers to some fundamental open questions in the field of bone mechanics and point out the areas that might still need further research.

6. Appendix

6.1. Differentiation between Tensile and Compressive Ultimate Strain Values

To differentiate the effect of tensile versus compressive post-yield behavior, a parameter study was performed on one specimen in which the ultimate strain of each of the trabecular or cortical tissue was parametrically varied in either tension or compression by 1 SD from the mean value, resulting in eight additional cases (**Table 6-1**).

These additional analyses indicated that the overall vertebral strength was dominated by the compressive post-yield behavior of each tissue (**Figure 6-1**). Increasing the cortical compressive ultimate strain from the -1 SD value (1.3%) to the +1 SD value (3.1%), with the cortical tensile ultimate strain (2.2%) and trabecular ultimate strain in tension and compression (8.8%) held constant, increased vertebral strength by about 6.7%, while increasing the cortical tensile ultimate strain from the -1 SD value (1.3%) to the +1 SD value (3.1%), with the cortical compressive ultimate strain (2.2%) and trabecular ultimate strain in tension and compression (8.8%) held constant, increased vertebral strength by only about 0.6%. Similarly, increasing the trabecular compressive ultimate strain from the -1 SD value (5.1%) to the +1 SD value (12.5%), with the trabecular tensile ultimate strain (8.8%) and cortical ultimate strain in tension and compression (2.2%) held constant, increased vertebral strength by about 7.1%, while increasing the trabecular tensile ultimate strain from the -1 SD value (5.1%) to the +1 SD value (12.5%), with the trabecular compressive ultimate strain (8.8%) and cortical ultimate strain in tension and compression (2.2%) held constant, increased vertebral strength by only about 0.3%.

Although previous studies have mostly focused on characterizing tissue tensile brittleness, our results suggest that vertebral strength is dominated by the compressive post-yield behavior of the tissue. The underlying mechanism could be related to the multi-scale nature of whole-bone failure:

bone tissue is stronger in compression; thus, it takes more load under compression upon yielding. Therefore, when the tissue loaded in compression fractures, there would be a greater reduction in overall strength compared to the tissue loaded in tension. Together these results might provide new insight into bone quality behavior and suggest that more experiments need to be done to better characterize the compressive failure strain of the bone tissue and its changes with aging, disease and treatment.

Table 6-1: Simulated tissue-level ultimate strain cases for tension versus compression comparison. The middle case in each "block" is the reference case (case 5 in **Table 2-1**) that was simulated before. Therefore, a total of 8 additional cases were defined to differentiate the effect of tensile versus compressive post-yield behavior.

	ε_{ult}^{trab}		$\varepsilon_{ult}^{cort.}$	
Case	**tension**	**compression**	**tension**	**compression**
A1	8.8	5.1	2.2	2.2
A2	8.8	8.8	2.2	2.2
A3	8.8	12.5	2.2	2.2
A4	5.1	8.8	2.2	2.2
A5	8.8	8.8	2.2	2.2
A6	12.5	8.8	2.2	2.2
A7	8.8	8.8	2.2	1.3
A8	8.8	8.8	2.2	2.2
A9	8.8	8.8	2.2	3.1
A10	8.8	8.8	1.3	2.2
A11	8.8	8.8	2.2	2.2
A12	8.8	8.8	3.1	2.2

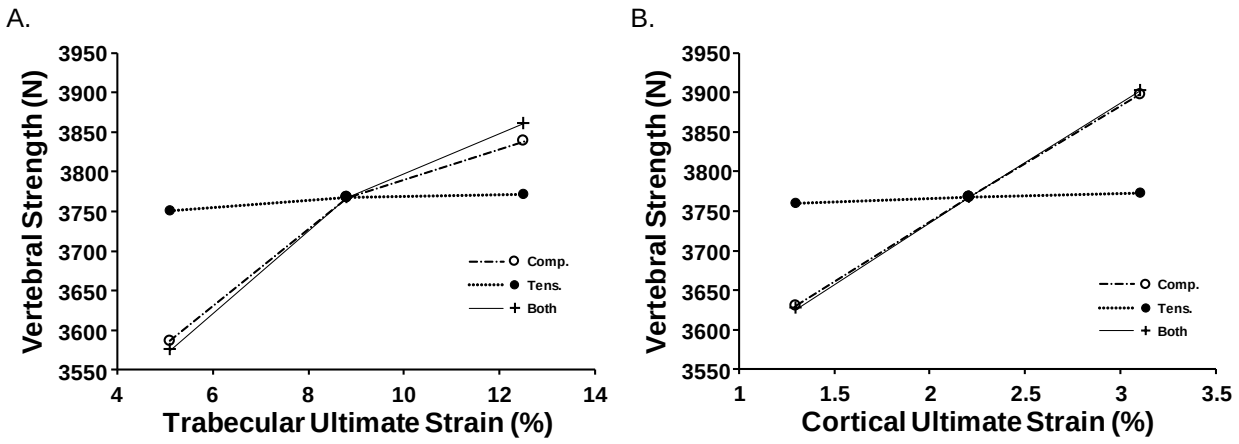

Figure 6-1: A) Effect of trabecular tensile and compressive ultimate strain on vertebral strength, for a fixed cortical ultimate strain value of 2.2% in tension and compression. B) Effect of cortical tensile and compressive ultimate strain on vertebral strength, for a fixed trabecular ultimate strain value of 8.8% in tension and compression.

6.2. Validation of FEA Methodology

To validate our FEA methodology, the FEA-estimated yield stress was compared against the corresponding experimental measurements for a subset of the specimens. The mechanical tests are described in details in a prior study [110]. Briefly, these tests were conducted using a servohydraulic load frame (858 Mini-Bionix, MTS, Eden Prairie, MN) using protocols to minimize the end-artifact effects [10]. Specimens were preconditioned to 0.1% strain, followed by destructive loading at 0.5% strain per second and the yield point was determined by the 0.2% offset technique [110].

For each anatomic site, the FEA-estimated yield stress was highly correlated with the experimental value (pooled R^2=0.97, **Figure 6-2**). No difference was found in the regression slope ($p > 0.5$) although the intercept of the regression was different across sites ($p < 0.0001$ for site).

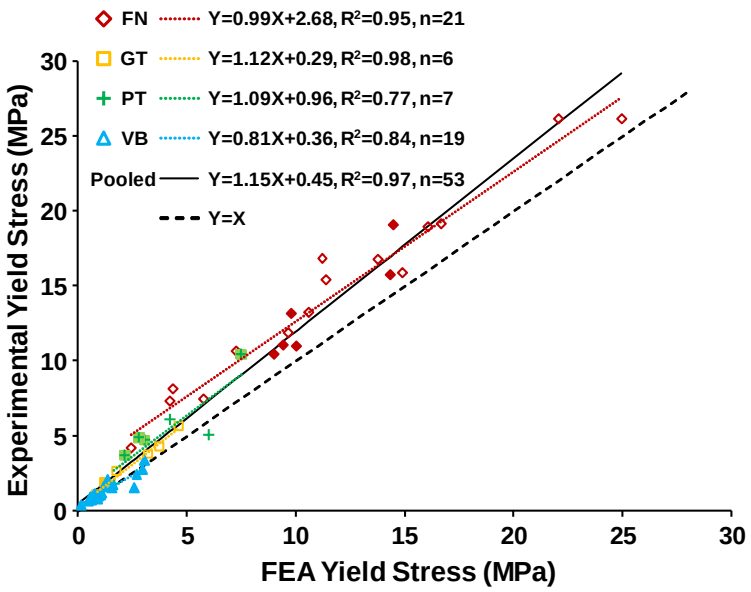

Figure 6-2: Experimental yield stress (biomechanical testing) versus finite element analysis yield stress for trabecular bone for a subset of the specimens (FN: Femoral Neck; GT: Greater Trochanter; PT: Proximal Tibia; VB: Vertebral Body); filled data were mechanically tested in tension; for these, the finite element analysis was also performed under tension.

7. References

[1] X. Feng, J.M. McDonald, Disorders of bone remodelling, Annu Rev Pathol. 6 (2011) 121–145. doi:10.1146/annurev-pathol-011110-130203.

[2] NIH, Osteoporosis Prevention, Diagnosis, and Therapy, J. Am. Med. Assoc. 285 (2001) 785–795.

[3] R. Burge, B. Dawson-Hughes, D.H. Solomon, J.B. Wong, A. King, A. Tosteson, Incidence and economic burden of osteoporosis-related fractures in the United States, 2005-2025, J. Bone Miner. Res. 22 (2007) 465–475. doi:10.1359/JBMR.061113.

[4] O. Johnell, J.A. Kanis, A. Odén, I. Sernbo, I. Redlund-Johnell, C. Petterson, C. De Laet, B. Jönsson, Mortality after osteoporotic fractures, Osteoporos. Int. 15 (2004) 38–42. doi:10.1007/s00198-003-1490-4.

[5] J.A. Kanis, L.J. Melton, C. Christiansen, C.C. Johnston, N. Khaltaev, The diagnosis of osteoporosis, J. Bone Miner. Res. 9 (1994) 1137–1141. doi:10.5124/jkma.2016.59.11.842.

[6] E.S. Siris, Y.T. Chen, T.A. Abbott, E. Barrett-Connor, P.D. Miller, L.E. Wehren, M.L. Berger, Bone mineral density thresholds for pharmacological intervention to prevent fractures, Arch. Intern. Med. 164 (2004) 1108–1112. doi:10.1001/archinte.164.10.1108.

[7] C.J. Hernandez, T.M. Keaveny, A biomechanical perspective on bone quality, Bone. 39 (2006) 1173–1181. doi:10.1016/j.bone.2006.06.001.

[8] I. Hvid, S.M. Bentzen, F. Linde, L. Mosekilde, B. Pongsoipetch, X-ray quantitative computed tomography: The relations to physical properties of proximal tibial trabecular bone specimens, J. Biomech. 22 (1989) 837–844. doi:10.1016/0021-9290(89)90067-5.

[9] J. Lotz, T. Gerhart, W. Hayes, Mechanical properties of trabecular bone from the proximal femur: a quantitative CT study, J. Comput. Assist. Tomogr. 14 (1990) 107–114. doi:10.1097/00004728-199001000-00020.

[10] D.L. Kopperdahl, T.M. Keaveny, Yield strain behavior of trabecular bone, J. Biomech. 31 (1998) 601–608. doi:10.1016/S0021-9290(98)00057-8.

[11] P. Brinckmann, M. Biggemann, D. Hilweg, Prediction of the compressive strength of human lumbar vertebrae, Clin. Biomech. 4 (1989) S1–S27. doi:10.1016/0268-0033(89)90071-5.

[12] S.M. Lang, D.D. Moyle, E.W. Berg, N. Detorie, A.T. Gilpin, N.J. Pappas, J.C. Reynolds,

M. Tkacik, R.L. Waldron, Correlation of mechanical properties of vertebral trabecular bone with equivalent mineral density as measured by computed tomography, J. Bone Jt. Surg. 70-A (1988) 1531–1538. doi:10.2106/00004623-198870100-00013.

[13] S.R. Cummings, D.B. Karpf, F. Harris, H.K. Genant, K. Ensrud, A.Z. LaCroix, D.M. Black, Improvement in spine bone density and reduction in risk of vertebral fractures during treatment with antiresorptive drugs, Am. J. Med. 112 (2002) 281–289. doi:10.1016/S0002-9343(01)01124-X.

[14] P.D. Delmas, How does antiresorptive therapy decrease the risk of fracture in women with osteoporosis?, Bone. 27 (2000) 1–3. doi:10.1016/S8756-3282(00)00301-X.

[15] G.L. Niebur, M.J. Feldstein, J.C. Yuen, T.J. Chen, T.M. Keaveny, High-resolution finite element models with tissue strength asymmetry accurately predict failure of trabecular bone, J. Biomech. 33 (2000) 1575–1583. doi:10.1016/S0021-9290(00)00149-4.

[16] W. Pistoia, B. van Rietbergen, A. Laib, P. Rüegsegger, High-Resolution Three-Dimensional-pQCT Images Can Be an Adequate Basis for In-Vivo μFE Analysis of Bone, J. Biomech. Eng. 123 (2001) 176–183. doi:10.1115/1.1352734.

[17] G. Bevill, S.K. Eswaran, A. Gupta, P. Papadopoulos, T.M. Keaveny, Influence of bone volume fraction and architecture on computed large-deformation failure mechanisms in human trabecular bone, Bone. 39 (2006) 1218–1225. doi:10.1016/j.bone.2006.06.016.

[18] L.J. Gibson, The mechanical behaviour of cancellous bone, J. Biomech. 18 (1985) 317–328. doi:10.1016/0021-9290(85)90287-8.

[19] R.W. McCalden, J.A. McGeough, M.B. Barker, C.M. Court-Brown, Age-Related Changes in the Tensile Properties of Cortical Bone. The Relative Importance of Changes in Porosity, Mineralization, and Microstructure., J. Bone Jt. Surg. 75-A (1993) 1193–1205.

[20] C.J. Hernandez, S.Y. Tang, B.M. Baumbach, P.B. Hwu, A.N. Sakkee, F. Van Der Ham, J. DeGroot, R.A. Bank, T.M. Keaveny, Trabecular microfracture and the influence of pyridinium and non-enzymatic glycation-mediated collagen cross-links, Bone. 37 (2005) 825–832. doi:10.1016/j.bone.2005.07.019.

[21] R. Carretta, E. Stussi, R. Muller, S. Lorenzetti, Within subject heterogeneity in tissue-level post- yield mechanical and material properties in human trabecular bone, J. Mech. Behav. Biomed. Mater. 24 (2013) 64–73. doi:10.1016/j.jmbbm.2013.04.014.

[22] R. Carretta, B. Luisier, D. Bernoulli, E. Stussi, R. Muller, S. Lorenzetti, Novel method to analyze post-yield mechanical properties at trabecular bone tissue level, J. Mech. Behav. Biomed. Mater. 20 (2013) 6–18. doi:10.1016/j.jmbbm.2012.12.003.

[23] E.F. Morgan, H.H. Bayraktar, O.C. Yeh, S. Majumdar, A. Burghardt, T.M. Keaveny, Contribution of inter-site variations in architecture to trabecular bone apparent yield strains, J. Biomech. 37 (2004) 1413–1420. doi:10.1016/j.jbiomech.2003.12.037.

[24] E.F. Morgan, H.H. Bayraktar, T.M. Keaveny, Trabecular bone modulus–density relationships depend on anatomic site, J. Biomech. 36 (2003) 897–904. doi:10.1016/S0021-9290(03)00071-X.

[25] S.J. Kaplan, W.C. Hayes, J.L. Stone, G.S. Beaupré, TENSILE STRENGTH OF BOVINE TRABECULAR BONE, J. Biomech. 18 (1985) 723–727. doi:10.1016/0021-9290(85)90027-2.

[26] J.L. Stone, G.S. Beaupre, W.C. Hayes, Multiaxial strength characteristics of trabecular bone, J. Biomech. 16 (1983) 743–752. doi:10.1016/0021-9290(83)90083-0.

[27] T.M. Keaveny, E.F. Wachtel, C.M. Ford, W.C. Hayes, Differences between the tensile and compressive strengths of bovine tibial trabecular bone depend on modulus, J. Biomech. 27 (1994) 1137–1146. doi:10.1016/0021-9290(94)90054-X.

[28] F. Linde, I. Hvid, THE EFFECT OF CONSTRAINT ON THE MECHANICAL BEHAVIOUR OF TRABECULAR BONE SPECIMENS, J. Biomech. 22 (1989) 485–490. doi:10.1016/0021-9290(89)90209-1.

[29] G. Bevill, S.K. Eswaran, F. Farahmand, T.M. Keaveny, The influence of boundary conditions and loading mode on high-resolution finite element-computed trabecular tissue properties, Bone. 44 (2009) 573–578. doi:10.1016/j.bone.2008.11.015.

[30] S.K. Eswaran, H.H. Bayraktar, M.F. Adams, A. Gupta, P.F. Hoffmann, D.C. Lee, P. Papadopoulos, T.M. Keaveny, The micro-mechanics of cortical shell removal in the human vertebral body, Comput. Methods Appl. Mech. Engrg. 196 (2007) 3025–3032. doi:10.1016/j.cma.2006.06.017.

[31] B.C. Bourne, M.C.H. Van Der Meulen, Finite element models predict cancellous apparent modulus when tissue modulus is scaled from specimen CT-attenuation, J. Biomech. 37 (2004) 613–621. doi:10.1016/j.jbiomech.2003.10.002.

[32] S.K. Easley, M.G. Jekir, A.J. Burghardt, M. Li, T.M. Keaveny, Contribution of the intra-specimen variations in tissue mineralization to PTH- and raloxifene-induced changes in stiffness of rat vertebrae, Bone. 46 (2010) 1162–1169. doi:10.1016/j.bone.2009.12.009.

[33] M.J. Jaasma, H.H. Bayraktar, G.L. Niebur, T.M. Keaveny, Biomechanical effects of intraspecimen variations in tissue modulus for trabecular bone, J. Biomech. 35 (2002) 237–246. doi:10.1016/S0021-9290(01)00193-2.

[34] S.K. Eswaran, A. Gupta, M.F. Adams, T.M. Keaveny, Cortical and Trabecular Load Sharing in the Human Vertebral Body, J. Bone Miner. Res. 21 (2006) 307–314. doi:10.1359/JBMR.051027.

[35] S.K. Eswaran, A. Gupta, T.M. Keaveny, Locations of bone tissue at high risk of initial failure during compressive loading of the human vertebral body, Bone. 41 (2007) 733–739. doi:10.1016/j.bone.2007.05.017.

[36] J. Homminga, B. Van-Rietbergen, E.M. Lochmüller, H. Weinans, F. Eckstein, R. Huiskes, The osteoporotic vertebral structure is well adapted to the loads of daily life, but not to infrequent "error" loads, Bone. 34 (2004) 510–516. doi:10.1016/j.bone.2003.12.001.

[37] H. Frei, T.R. Oxland, L.P. Nolte, Thoracolumbar spine mechanics contrasted under compression and shear loading, J. Orthop. Res. 20 (2002) 1333–1338. doi:10.1016/S0736-0266(02)00058-X.

[38] H.H. Bayraktar, E.F. Morgan, G.L. Niebur, G.E. Morris, E.K. Wong, T.M. Keaveny, Comparison of the elastic and yield properties of human femoral trabecular and cortical bone tissue, J. Biomech. 37 (2004) 27–35. doi:10.1016/S0021-9290(03)00257-4.

[39] B. van Rietbergen, H. Weinans, R. Huiskes, A. Odgaardt, A new method to determine trabecular bone elastic properties and loading using micromechanical finite-elements models, J. Biomech. 28 (1995) 69–81. doi:10.1016/0021-9290(95)80008-5.

[40] J. Homminga, H. Weinans, W. Gowin, D. Felsenberg, R. Huiskes, Osteoporosis changes the amount of vertebral trabecular bone at risk of fracture but not the vertebral load distribution, Spine (Phila. Pa. 1976). 26 (2001) 1555–1560. doi:10.1097/00007632-200107150-00010.

[41] J.M. Buckley, K. Loo, J. Motherway, Comparison of quantitative computed tomography-based measures in predicting vertebral compressive strength, Bone. 40 (2007) 767–774. doi:10.1016/j.bone.2006.10.025.

[42] Y. Chevalier, M. Charlebois, D. Pahr, P. Varga, P. Heini, E. Schneider, P. Zysset, A patient-specific finite element methodology to predict damage accumulation in vertebral bodies under axial compression, sagittal flexion and combined loads, Comput. Methods Biomech. Biomed. Engin. 11 (2008) 477–487. doi:10.1080/10255840802078022.

[43] R.P. Crawford, C.E. Cann, T.M. Keaveny, Finite element models predict in vitro vertebral body compressive strength better than quantitative computed tomography, Bone. 33 (2003) 744–750. doi:10.1016/S8756-3282(03)00210-2.

[44] C. Graeff, Y. Chevalier, M. Charlebois, P. Varga, D. Pahr, T.N. Nickelsen, M.M. Morlock,

C.C. Glüer, P.K. Zysset, Improvements in vertebral body strength under teriparatide treatment assessed in vivo by finite element analysis: Results from the EUROFORS study, J. Bone Miner. Res. 24 (2009) 1672–1680. doi:10.1359/jbmr.090416.

[45] L.J. Melton, B.L. Riggs, T.M. Keaveny, S.J. Achenbach, P.F. Hoffmann, J.J. Camp, P.A. Rouleau, M.L. Bouxsein, S. Amin, E.J. Atkinson, R.A. Robb, S. Khosla, Structural Determinants of Vertebral Fracture Risk, J. Bone Miner. Res. 22 (2007) 1885–1892. doi:10.1359/jbmr.070728.

[46] F.J. Hou, S.M. Lang, S.J. Hoshaw, D.A. Reimann, D.P. Fyhrie, Human vertebral body apparent and hard tissue stiffness, J. Biomech. 31 (1998) 1009–1015. doi:10.1016/S0021-9290(98)00110-9.

[47] J. Kabel, B. Van Rietbergen, M. Dalstra, A. Odgaard, R. Huiskes, The role of an effective isotropic tissue modulus in the elastic properties of cancellous bone, J. Biomech. 32 (1999) 673–680. doi:10.1016/S0021-9290(99)00045-7.

[48] S. Nagaraja, T.L. Couse, R.E. Guldberg, Trabecular bone microdamage and microstructural stresses under uniaxial compression, J. Biomech. 38 (2005) 707–716. doi:10.1016/j.jbiomech.2004.05.013.

[49] X. Shi, X.S. Liu, X. Wang, X.E. Guo, G.L. Niebur, Effects of trabecular type and orientation on microdamage susceptibility in trabecular bone, Bone. 46 (2010) 1260–1266. doi:10.1016/j.bone.2010.02.005.

[50] M.F. Adams, H.H. Bayraktar, T.M. Keaveny, P. Papadopoulos, Ultrascalable Implicit Finite Element Analysis in Solid Mechanics with over a Half a Billion Degrees of Freedom, in: Proc. 2004 ACM/IEEE Conf. Supercomput., Washington, DC, 2004. doi:10.1109/SC.2004.62.

[51] P. Arbenz, G.H. VanLenthe, U. Mennel, R. Muller, M. Sala, A scalable multi-level preconditioner for matrix-free micro-finite element analysis of human bone structures, Int. J. Numer. Methods Eng. 73 (2008) 927–947. doi:10.1002/nme.

[52] M.F. Adams, H.H. Bayraktar, T.M. Keaveny, P. Papdopoulos, Applications of Algebraic Multigrid to Large-Scale Finite Element Analysis of Whole Bone Micro-Mechanics on the IBM SP, in: Proc. 2003 ACM/IEEE Conf. Supercomput., Phoenix, AZ, 2003. doi:10.1109/SC.2003.10050.

[53] J.S. Stölken, J.H. Kinney, On the importance of geometric nonlinearity in finite-element simulations of trabecular bone failure, Bone. 33 (2003) 494–504. doi:10.1016/S8756-3282(03)00214-X.

[54] S. Nawathe, H. Yang, A.J. Fields, M.L. Bouxsein, T.M. Keaveny, Theoretical effects of fully ductile versus fully brittle behaviors of bone tissue on the strength of the human proximal femur and vertebral body, J. Biomech. 48 (2015) 1264–1269. doi:10.1016/j.jbiomech.2015.02.066.

[55] S. Nawathe, H. Akhlaghpour, M.L. Bouxsein, T.M. Keaveny, Microstructural Failure Mechanisms in the Human Proximal Femur for Sideways Fall Loading, J. BONE Miner. Res. 29 (2014) 507–515. doi:10.1002/jbmr.2033.

[56] S. Nawathe, F. Juillard, T.M. Keaveny, Theoretical bounds for the influence of tissue-level ductility on the apparent-level strength of human trabecular bone, J. Biomech. 46 (2013) 1293–1299. doi:10.1016/j.jbiomech.2013.02.011.

[57] A.J. Fields, S. Nawathe, S.K. Eswaran, M.G. Jekir, M.F. Adams, P. Papadopoulos, T.M. Keaveny, Vertebral Fragility and Structural Redundancy, J. BONE Miner. Res. 27 (2012) 2152–2158. doi:10.1002/jbmr.1664.

[58] D.L. Bartel, D.T. Davy, T.M. Keaveny, Orthopaedic Biomechanics Mechanics and Design in Musculoskeletal Systems, Pearson Education, Upper Saddle River, New Jersey, 2006.

[59] B.A. Christiansen, D.L. Kopperdahl, P.K. Douglas, T.M. Keaveny, M.L. Bouxsein, Mechanical contributions of the cortical and trabecular compartments contribute to differences in age-related changes in vertebral body strength in men and women assessed by QCT-based finite element analysis, J. Bone Miner. Res. 26 (2011) 974–983. doi:10.1002/jbmr.287.

[60] D.P. Fyhrie, M.B. Schaffler, Failure mechanisms in human vertebral cancellous bone, Bone. 15 (1994) 105–109. doi:10.1016/8756-3282(94)90900-8.

[61] O.C. Yeh, T.M. Keaveny, Roles of microdamage and microfracture in the mechanical behavior of trabecular bone, in: 46th Annu. Meet. Orthop. Res. Soc., Orlando, Florida, 2000.

[62] L. Mosekilde, L. Mosekilde, Sex differences in age-related changes in vertebral body size, density and biomechanical competence in normal individuals, Bone. 11 (1990) 67–73. doi:10.1016/8756-3282(90)90052-Z.

[63] D.L. Kopperdahl, T. Aspelund, P.F. Hoffmann, S. Sigurdsson, K. Siggeirsdottir, T.B. Harris, V. Gudnason, T.M. Keaveny, Assessment of incident spine and hip fractures in women and men using finite element analysis of CT scans, J. Bone Miner. Res. 29 (2014) 570–580. doi:10.1002/jbmr.2069.

[64] B. van Rietbergen, H. Weinans, R. Huiskes, A. Odgaard, A new method to determine trabecular bone elastic properties and loading using micromechanical finite-element

models, J. Biomech. 28 (1995) 69–81. doi:10.1016/0021-9290(95)80008-5.

[65] A.J. Fields, S.K. Eswaran, M.G. Jekir, T.M. Keaveny, Role of Trabecular Microarchitecture in Whole-Vertebral Body Biomechanical Behavior, J. BONE Miner. Res. 24 (2009) 1523–1530. doi:10.1359/JBMR.090317.

[66] P.H.F. Nicholson, X.G. Cheng, G. Lowet, S. Boonen, M.W.J. Davie, J. Dequeker, G. Van Der Perre, Structural and material mechanical properties of human vertebral cancellous bone, Med. Eng. Phys. 19 (1997) 729–737. doi:10.1016/S1350-4533(97)00030-1.

[67] J.Y. Rho, T.Y. Tsui, G.M. Pharr, Elastic properties of human cortical and trabecular lamellar bone measured by nanoindentation, Biomaterials. 18 (1997) 1325–1330. doi:10.1016/S0142-9612(97)00073-2.

[68] C.E. Hoffler, K.E. Moore, K. Kozloff, P.K. Zysset, M.B. Brown, S.A. Goldstein, Heterogeneity of bone lamellar-level elastic moduli, Bone. 26 (2000) 603–9. doi:10.1016/S8756-3282(00)00268-4.

[69] J.Y. Rho, M.E. Roy, T.Y. Tsui, G.M. Pharr, Elastic properties of microstructural components of human bone tissue as measured by nanoindentation, J. Biomed. Mater. Res. 45 (1999) 48–54. doi:10.1002/(SICI)1097-4636(199904)45:1<48::AID-JBM7>3.0.CO;2-5.

[70] U. Wolfram, H.J. Wilke, P.K. Zysset, Valid μ finite element models of vertebral trabecular bone can be obtained using tissue properties measured with nanoindentation under wet conditions, J. Biomech. 43 (2010) 1731–1737. doi:10.1016/j.jbiomech.2010.02.026.

[71] H. Giambini, H.J. Wang, C. Zhao, Q. Chen, A. Nassr, K.N. An, Anterior and posterior variations in mechanical properties of human vertebrae measured by nanoindentation, J. Biomech. 46 (2013) 456–461. doi:10.1016/j.jbiomech.2012.11.008.

[72] A.J.C. Ladd, J.H. Kinney, D.L. Haupt, S. a Goldstein, Finite-Element Modeling of Trabecular Bone: Comparison with Mechanical Testing and Determination of Tissue Modulus, J. Orthop. Res. 16 (1998) 622–628. doi:10.1002/jor.1100160516.

[73] C.R. Jacobs, B.R. Davis, C.J. Rieger, J.J. Francis, M. Saad, D.P. Fyhrie, The impact of boundary conditions and mesh size on the accuracy of cancellous bone tissue modulus determination using large-scale finite-element modeling, J. Biomech. 32 (1999) 1159–1164. doi:10.1016/S0021-9290(99)00115-3.

[74] T.M. Keaveny, T.P. Pinilla, R.P. Crawford, D.L. Kopperdahl, A. Lou, Systematic and random errors in compression testing of trabecular bone, J. Orthop. Res. 15 (1997) 101–110. doi:10.1002/jor.1100150115.

[75] A. Odgaard, F. Linde, The underestimation of Young's modulus in compressive testing of cancellous bone specimens, J. Biomech. 24 (1991) 691–698. doi:10.1016/0021-9290(91)90333-I.

[76] T.M. Keaveny, R.E. Borchers, L.J. Gibson, W.C. Hayes, Theoretical analysis of the experimental artifact in trabecular bone compressive modulus, J. Biomech. 26 (1993) 599–607. doi:10.1016/0021-9290(93)90021-6.

[77] H. Yang, S. Nawathe, A.J. Fields, T.M. Keaveny, Micromechanics of the human vertebral body for forward flexion, J. Biomech. 45 (2012) 2142–2148. doi:10.1016/j.jbiomech.2012.05.044.

[78] P. Zioupos, R. Cook, A.M. Coats, Bone quality issues and matrix properties in OP cancellous bone, in: J. Hammer, M. Nerlich, S. Dendorfer (Eds.), Med. Meets Eng., IOS Press, Amsterdam, Netherlands, 2008: pp. 238–45.

[79] L.M. McNamara, A.G.H. Ederveen, C.G. Lyons, C. Price, M.B. Schaffler, H. Weinans, P.J. Prendergast, Strength of cancellous bone trabecular tissue from normal, ovariectomized and drug-treated rats over the course of ageing, Bone. 39 (2006) 392–400. doi:10.1016/j.bone.2006.02.070.

[80] L.M. McNamara, P.J. Prendergast, M.B. Schaffler, Bone tissue material properties are altered during osteoporosis, J. Musculoskelet Neuronal Interact. 5 (2005) 342–343.

[81] B. Busse, M. Hahn, M. Soltau, J. Zustin, K. Püschel, G.N. Duda, M. Amling, Increased calcium content and inhomogeneity of mineralization render bone toughness in osteoporosis: Mineralization, morphology and biomechanics of human single trabeculae, Bone. 45 (2009) 1034–1043. doi:10.1016/j.bone.2009.08.002.

[82] R.E. Guldberg, S.J. Hollister, G.T. Charras, The Accuracy of Digital Image-Based Finite Element Models, J. Biomech. Eng. 120 (1998) 289–295. doi:10.1115/1.2798314.

[83] G.L. Niebur, J.C. Yuen, A.C. Hsia, T.M. Keaveny, Convergence Behavior of High-Resolution Finite Element Models of Trabecular Bone, J. Biomech. Eng. 121 (1999) 629. doi:10.1115/1.2800865.

[84] F. Cosman, S.J. de Beur, M.S. LeBoff, E.M. Lewiecki, B. Tanner, S. Randall, R. Lindsay, Clinician's Guide to Prevention and Treatment of Osteoporosis, Osteoporos. Int. 25 (2014) 2359–2381. doi:10.1007/s00198-014-2794-2.

[85] J. Zhang, E. Delzell, H. Zhao, A.J. Laster, K.G. Saag, M.L. Kilgore, M.A. Morrisey, N.C. Wright, H. Yun, J.R. Curtis, Central DXA utilization shifts from office-based to hospital-based settings among medicare beneficiaries in the wake of reimbursement changes, J. Bone

Miner. Res. 27 (2012) 858–864. doi:10.1002/jbmr.1534.

[86] C.M. Langton, S.B. Palmer, R.W. Porter, The measurement of broadband ultrasonic attenuation in cancellous bone, Eng. Med. 13 (1984) 89–91. doi:10.1243/EMED_JOUR_1984_013_022_02.

[87] P. Laugier, Instrumentation for in vivo ultrasonic characterization of bone strength, IEEE Trans. Ultrason. Ferroelectr. Freq. Control. 55 (2008) 1179–1196. doi:10.1109/TUFFC.2008.782.

[88] P. Laugier, Quantitative Ultrasound Instrumentation for Bone In Vivo Characterization, in: P. Laugier, G. Haïat (Eds.), Bone Quant. Ultrasound, Springer, Dordrecht, 2011: pp. 47–71. doi:10.1007/978-94-007-0017-8_3.

[89] R. Barkmann, C.-C. Glüer, Clinical Applications, in: P. Laugier, G. Haïat (Eds.), Bone Quant. Ultrasound, Springer, Dordrecht, 2011: pp. 73–81. doi:10.1007/978-94-007-0017-8_4.

[90] C.E. Waud, R. Lew, D.T. Baran, The relationship between ultrasound and densitometric measurements of bone mass at the calcaneus in women, Calcif. Tissue Int. 51 (1992) 415–418. doi:10.1007/BF00296673.

[91] P. Laugier, P. Droin, A.M. Laval-Jeantet, G. Berger, In vitro assessment of the relationship between acoustic properties and bone mass density of the calcaneus by comparison of ultrasound parametric imaging and quantitative computed tomography, Bone. 20 (1997) 157–165. doi:10.1016/S8756-3282(96)00347-X.

[92] B. Cortet, N. Boutry, P. Dubois, I. Legroux-Gérot, A. Corten, X. Marchandise, Does Quantitative Ultrasound of Bone Reflect More Bone Mineral Density Than Bone Microarchitecture?, Calcif. Tissue Int. 74 (2004) 60–67. doi:10.1007/s00223-002-2113-3.

[93] S. Chaffaí, F. Peyrin, S. Nuzzo, R. Porcher, G. Berger, P. Laugier, Ultrasonic characterization of human cancellous bone using transmission and backscatter measurements: Relationships to density and microstructure, Bone. 30 (2002) 229–237. doi:10.1016/S8756-3282(01)00650-0.

[94] H. Trebacz, A. Natali, Ultrasound velocity and attenuation in cancellous bone samples from lumbar vertebra and calcaneus, Osteoporos. Int. 9 (1999) 99–105. doi:10.1007/s001980050121.

[95] P.H.F. Nicholson, R. Müller, X.G. Cheng, P. Rüegsegger, G. Van Der Perre, J. Dequeker, S. Boonen, Quantitative ultrasound and trabecular architecture in the human calcaneus, J. Bone Miner. Res. 16 (2001) 1886–1892. doi:10.1359/jbmr.2001.16.10.1886.

[96] K. a. Wear, S. Nagaraja, M.L. Dreher, S.L. Gibson, Relationships of quantitative ultrasound parameters with cancellous bone microstructure in human calcaneus in vitro, J. Acoust. Soc. Am. 131 (2012) 1605–1612. doi:10.1121/1.3672701.

[97] M.L. Bouxsein, S.E. Radloff, Quantitative ultrasound of the calcaneus reflects the mechanical properties of calcaneal trabecular bone, J. Bone Miner. Res. 12 (1997) 839–846. doi:10.1359/jbmr.1997.12.5.839.

[98] K.A. Wear, S. Nagaraja, M.L. Dreher, S. Sadoughi, S. Zhu, T.M. Keaveny, Relationships among ultrasonic and mechanical properties of cancellous bone in human calcaneus in vitro, Bone. 103 (2017) 93–101. doi:10.1016/j.bone.2017.06.021.

[99] C.M. Langton, C.F. Njeh, R. Hodgskinson, J.D. Currey, Prediction of mechanical properties of the human calcaneus by broadband ultrasonic attenuation, Bone. 18 (1996) 495–503. doi:10.1016/8756-3282(96)00086-5.

[100] M.A. Hakulinen, J.S. Day, J. Töyräs, M. Timonen, H. Kröger, H. Weinans, I. Kiviranta, J.S. Jurvelin, Prediction of density and mechanical properties of human trabecular bone in vitro by using ultrasound transmission and backscattering measurements at 0.2-6.7 MHz frequency range, Phys. Med. Biol. 50 (2005) 1629–1642. doi:10.1088/0031-9155/50/8/001.

[101] T. Hildebrand, A. Laib, R. Müller, J. Dequeker, P. Rüegsegger, Direct Three-Dimensional Morphometric Analysis of Human Cancellous Bone: Microstructural Data from Spine, Femur, Iliac Crest, and Calcaneus, J. Bone Miner. Res. 14 (2009) 1167–1174. doi:10.1359/jbmr.1999.14.7.1167.

[102] M. Amling, S. Herden, M. Pösl, M. Hahn, H. Ritzel, G. Delling, Heterogeneity of the Skeleton: Comparison of the Trabecular Microarchitecture of the Spine, the Iliac Crest, the Femur, and the Calcaneus, J. Bone Miner. Res. 11 (1996) 36–45. doi:10.1002/jbmr.5650110107.

[103] T.M. Link, S. Majumdar, P. Augat, J.C. Lin, D. Newitt, Y. Lu, N.E. Lane, H.K. Genant, In vivo high resolution MRI of the calcaneus: Differences in trabecular structure in osteoporosis patients, J. Bone Miner. Res. 13 (1998) 1175–1182. doi:10.1359/jbmr.1998.13.7.1175.

[104] L. Duchemin, V. Bousson, C. Raossanaly, C. Bergot, J.D. Laredo, W. Skalli, D. Mitton, Prediction of mechanical properties of cortical bone by quantitative computed tomography, Med. Eng. Phys. 30 (2008) 321–328. doi:10.1016/j.medengphy.2007.04.008.

[105] X. Ouyang, K. Selby, P. Lang, K. Engelke, C. Klifa, B. Fan, F. Zucconi, G. Hottya, M. Chen, S. Majumdar, H.K. Genant, High resolution magnetic resonance imaging of the calcaneus: Age- related changes in trabecular structure and comparison with dual X-ray

absorptiometry measurements, Calcif. Tissue Int. 60 (1997) 139–147. doi:10.1007/s002239900204.

[106] E. Mittra, C. Rubin, B. Gruber, Y.X. Qin, Evaluation of trabecular mechanical and microstructural properties in human calcaneal bone of advanced age using mechanical testing, μCT, and DXA, J. Biomech. 41 (2008) 368–375. doi:10.1016/j.jbiomech.2007.09.003.

[107] G. Diederichs, T.M. Link, M. Kentenich, K. Schwieger, M.B. Huber, A.J. Burghardt, S. Majumdar, P. Rogalla, A.S. Issever, Assessment of trabecular bone structure of the calcaneus using multi-detector CT: Correlation with microCT and biomechanical testing, Bone. 44 (2009) 976–983. doi:10.1016/j.bone.2009.01.372.

[108] H. Follet, K. Bruyère-Garnier, F. Peyrin, J.P. Roux, M.E. Arlot, B. Burt-Pichat, C. Rumelhart, P.J. Meunier, Relationship between compressive properties of human os calcis cancellous bone and microarchitecture assessed from 2D and 3D synchrotron microtomography, Bone. 36 (2005) 340–351. doi:10.1016/j.bone.2004.10.011.

[109] J.D. Currey, Power law models for the mechanical properties of cancellous bone, Eng. Med. 15 (1986) 153–154. doi:10.1243/EMED_JOUR_1986_015_039_02.

[110] E.F. Morgan, T.M. Keaveny, Dependence of yield strain on anatomic site for human trabecular bone, J. Biomech. 34 (2001) 569–577. doi:10.1016/S0021-9290(01)00011-2.

[111] P. Papadopoulos, J. Lu, A general framework for the numerical solution of problems in finite elasto-plasticity, Comput. Methods Appl. Mech. Engrg. 159 (1998) 1–18. doi:10.1016/S0045-7825(98)80101-1.

[112] J.C. Rice, S.C. Cowin, J.A. Bowman, On the dependence of the elasticity and strength of cancellous bone on apparent density, J. Biomech. 21 (1988) 155–168. doi:10.1016/0021-9290(88)90008-5.

[113] M.L. Bouxsein, A.C. Courtney, W.C. Hayes, Ultrasound and densitometry of the calcaneus correlate with the failure loads of cadaveric femurs, Calcif. Tissue Int. 56 (1995) 99–103. doi:10.1007/BF00296338.

[114] W.C. Graafmans, A. V. Lingen, M.E. Ooms, P.D. Bezemer, P. Lips, Ultrasound measurements in the calcaneus: Precision and its relation with bone mineral density of the heel, hip, and lumbar spine, Bone. 19 (1996) 97–100. doi:10.1016/8756-3282(96)00134-2.

[115] R. Eastell, S.L. Cedel, H.W. Wahner, B.L. Riggs, L.J. Melton, Classification of vertebral fractures, J. Bone Miner. Res. 6 (1991) 207–215. doi:10.1002/jbmr.5650060302.